

New Results from a Near-Infrared Search for Hidden Broad-Line Regions in Ultraluminous Infrared Galaxies.

Sylvain Veilleux^{1,2}, D. B. Sanders³, and D.-C. Kim⁴

ABSTRACT

This paper reports the latest results from a near-infrared search for hidden broad-line regions (BLRs: $\Delta V_{\text{FWHM}} \gtrsim 2,000 \text{ km s}^{-1}$) in ultraluminous infrared galaxies (ULIGs). The new sample contains thirty-nine ULIGs from the 1-Jy sample selected for their lack of BLRs at optical wavelengths. Broad Pa α emission is detected for the first time in two sources—F05189–2524 and F13305–1739⁵. Broad Pa α emission may also be present in three other sources—F13443+0802 SW, F14394+5332, and F16156+0146—but new data are needed to make sure that H₂ $\lambda\lambda 1.8665, 1.8721$ are not contributing to this excess emission. The [Si VI] feature, a strong indicator of AGN activity, appears to be present in one object—F13305–1739—and perhaps also in Mrk 273 and F13454–2956. In addition, the presence of a hidden BLR is confirmed in the lower luminosity source F11058–1131.

The results from this new study are combined with those from our previously published survey (Veilleux, Sanders, & Kim 1997b) to produce a large database on 64 (non-Seyfert 1) ULIGs from the 1-Jy sample. All of the galaxies with strong evidence for a hidden BLR at near-infrared wavelengths present an optical Seyfert 2 spectrum. Overall, at least 50% (and perhaps up to 70%) of the optical Seyfert 2 galaxies in the combined sample present either a BLR or strong [Si VI] emission. In contrast, none of the 41 optically classified LINERs and H II galaxies in the sample shows any obvious signs of an energetically important AGN. Galaxies with ‘warm’ *IRAS* colors ($f_{25}/f_{60} \gtrsim 0.2$)⁶ show a tendency to harbor obscured BLRs in the near-infrared and to have large Pa α -to-infrared luminosity ratios. These results support those of our earlier survey and suggest that the screen of dust in most ‘warm’ Seyfert 2 galaxies is optically *thin* at 2 μm .

¹Department of Astronomy, University of Maryland, College Park, MD 20742; E-mail: veilleux@astro.umd.edu

²Visiting Astronomer at the United Kingdom Infrared Telescope, which is operated by the Royal Observatory Edinburgh on behalf of the U.K. Science and Engineering Research Council

³Institute for Astronomy, University of Hawaii, Honolulu, HI 96822; E-mail: sanders@ifa.hawaii.edu

⁴Infrared Processing and Analysis Center, California Institute of Technology, Pasadena, CA 91125; E-mail: kim@ipac.caltech.edu

⁵Object names that begin with ‘F’ are sources identified in the *IRAS* Faint Source Catalog, Version 2 (FSC: Moshir et al 1992)

⁶The quantities f_{25} , f_{60} are the *IRAS* flux densities in Jy at 25 μm and 60 μm , respectively.

When the results from this near-infrared survey are combined with those from a recent optical spectroscopic study of the entire 1-Jy sample of 118 ULIGs (Veilleux, Kim, & Sanders 1999), we find that the fraction of all ULIGs with optical or near-infrared signs of genuine AGN activity (either a BLR or [Si VI] emission) is at least 20 – 25%, but reaches 35 – 50% for objects with $L_{\text{ir}} > 10^{12.3} L_{\odot}$. Comparisons of the dereddened emission-line luminosities of the optical or obscured BLRs detected in the ULIGs of the 1-Jy sample with those of optical quasars indicate that the obscured AGN/quasar in ULIGs is the main source of energy in at least 15 – 25% of all ULIGs in the 1-Jy sample. This fraction is closer to 30 – 50% among ULIGs with $L_{\text{ir}} > 10^{12.3} L_{\odot}$. These results are compatible with those from recent mid-infrared spectroscopic surveys carried out with *ISO*.

Subject headings: infrared: galaxies – galaxies: active – galaxies: Seyfert – galaxies: starburst

1. Introduction

In Veilleux, Sanders, & Kim (1997b; hereafter VSK), a near-infrared search for obscured broad-line regions (BLRs) and [Si VI] emission feature was carried out in a set of twenty-five ULIGs selected from the *IRAS* 1-Jy survey of 118 ULIGs (Kim & Sanders 1998). Prior to selecting their set of 25 objects, VSK excluded the $\sim 10\%$ of the 118 galaxies that already were known optically to show direct signs of quasar activity, i.e. optically classified as Seyfert 1. Broad ($\Delta V_{\text{FWHM}} \gtrsim 2,000 \text{ km s}^{-1}$) infrared recombination lines were detected in 5 (possibly 8) of the 10 optically classified Seyfert 2 galaxies in the sample. The high-ionization [Si VI] feature ($\chi = 164 \text{ eV}$), a clear signature of an AGN, was detected in 3 or 4 of these Seyfert 2 galaxies. Interestingly, all 6 of the ‘warm’ ($f_{25}/f_{60} > 0.2$) optically classified Seyfert 2 galaxies in their sample showed either obscured BLRs or [Si VI] emission at near-infrared wavelengths, as well as large $\text{Pa}\alpha$ -to-infrared luminosity ratios, strongly suggesting that the screen of dust obscuring the cores of these ULIGs is optically thin at $2 \mu\text{m}$. In contrast, no obvious signs of an obscured BLR or strong [Si VI] emission were detected in any of the 15 optically classified LINERs and H II galaxies in sample of VSK. The obscured BLRs detected in the Seyfert 2 galaxies were found to have dereddened broad-line luminosities which are similar to those of optically selected quasars of comparable bolometric luminosity. This result was used by VSK to argue that most of the bolometric luminosity in these broad-line objects is powered by the same mechanism as that in optical quasars, namely mass accretion onto a supermassive black hole.

The results of VSK rely on very small numbers of objects (e.g., there were only 10 optically classified Seyfert 2 galaxies in their sample). Their conclusions are therefore affected by large statistical uncertainties. For this reason and because of the success of this initial survey, another set of 39 objects from the 1-Jy sample was observed using the same techniques as VSK (cf. Table

1). F11058–1131, a luminous infrared galaxy (LIG) with $\log(L_{\text{IR}}/L_{\odot}) = 11.3$, was also observed to test the reported detection of broad polarized emission lines in this object (Young et al. 1993). The present paper describes the results of this new study and combines them with the earlier data of VSK to produce a sample of 64 ULIGs and 1 LIG which comprises 23 optically classified Seyfert 2s, 25 LINERs, 16 H II galaxies, and one object with undetermined optical spectral type.

Section 2 of this paper describes the techniques used to acquire and analyze the new data. The results of the new survey are presented in Section 3 and combined with the results of VSK. In Section 4, the combined sample is used to test the conclusions of VSK. The conclusions from this analysis are summarized in Section 5 and combined with our recent optical spectroscopic results. This allows us to make statistically meaningful statements about the fraction of ULIGs which harbor a quasar, how this fraction varies with infrared luminosity and optical spectral type, and whether the quasars detected at optical and near-infrared wavelengths are energetically significant. A separate discussion of the emission-line properties of each object in the new sample, with particular emphasis on the presence or absence of broad components in the profiles of the infrared hydrogen recombination lines, is presented in an Appendix. We adopt $H_0 = 75 \text{ km s}^{-1} \text{ Mpc}^{-1}$ and $q_0 = 0$ throughout this paper.

2. Observations and Data Analysis

To allow direct comparisons with the results of VSK, all of the new data were acquired, reduced and analyzed using the same procedures as VSK (see also Goodrich et al. 1994 and Veilleux, Goodrich, & Hill 1997a). All of these data were obtained with CGS4 on UKIRT (Mountain et al. 1990). A summary of the observations is presented in Table 2. The 256×256 InSb array was used in conjunction with the 300 mm focal length camera and the 75 l/mm grating. The slit width and pixel scale were $1.''2$. All of the spectra were obtained under photometric conditions. However, as described in VSK, the absolute fluxes derived from these spectra are sensitive to slit losses, seeing, centering errors, and guiding effects. The line fluxes listed in Table 3 have been corrected for slit losses (based on seeing measurements taken throughout the night) but not for the other effects. This source of errors is estimated to be less than about 50%. A one-pixel ($1.''2$) extraction window was used to transform the long-slit data into one-dimensional spectra.

3. Results

The reduced spectra are presented in Figure 1 and discussed individually in the Appendix. Following the same format as in VSK, Table 3 lists the fluxes, equivalent widths, and line widths of the emission lines detected in these spectra. Also listed in this table are the intensities of $H\alpha$ and $H\beta$, the line widths of $[\text{O III}] \lambda 0.5007$ and the color excess, $E(B - V)$, determined from the optical emission-line flux ratios. Unless otherwise noted, these measurements were taken from Kim

et al. (1995), Kim, Veilleux, & Sanders (1998), Veilleux et al. (1995), or Veilleux, Kim, & Sanders (1999; hereafter VSK). The last two columns of Table 3 present the color excesses determined from the infrared emission-line flux ratios and based on the intrinsic flux ratios and extinction coefficients of Veilleux et al. (1997a; their Table 2).

As found by VSK, the spectra of ULIGs are characterized by strong Pa α emission and weaker lines from H₂. Weak emission from H₂ 1–0 S(5) λ 1.835, 1–0 S(2) λ 2.033, and 2–1 S(3) λ 2.073, and from Br γ λ 2.166, Br δ λ 1.945, Br ϵ λ 1.817, and He I λ 2.058 is also visible in some galaxies (cf. Table 3). Figure 2 shows the distributions of the intensities of H₂ 1–0 S(3) λ 1.958 (possibly blended with [Si VI] λ 1.962; see below) and H₂ 1–0 S(1) λ 2.122 relative to narrow Pa α as a function of optical spectral types. Ratios from the combined set of objects in VSK and the present sample are presented. This figure indicates that the H₂ emission in optical H II region-like galaxies is generally weaker than in optically classified LINERs or Seyfert 2s. The average H₂ 1–0 S(3) λ 1.958/Pa α ratios are 0.13, 0.23, and 0.32 for the H II galaxies (14 objects), LINERs (24) and Seyfert 2 galaxies (17), respectively. The average H₂ 1–0 S(1) λ 2.122/Pa α ratios are 0.11, 0.20, and 0.20 for the H II galaxies (8 objects), LINERs (15) and Seyfert 2 galaxies (10), respectively. Kolmogorov-Smirnov (K-S) tests confirm that the difference between the H II galaxies and the other types of objects is significant. The H₂ λ 1.958 and λ 2.122 luminosities in the combined sample of galaxies range from $5 \times 10^6 L_{\odot}$ to $3 \times 10^8 L_{\odot}$. These luminosities translate into hot H₂ masses of order 10,000–500,000 M_{\odot} if the hot H₂ molecules are thermalized at T = 2,000 K (Scoville et al. 1982).

There are only two strong cases for broad ($\Delta V_{\text{FWHM}} \gtrsim 2,000 \text{ km s}^{-1}$) line emission in the new sample of ULIGs: F05189–2524 and F13305–1739. We also detect very broad ($\Delta V_{\text{FWHM}} \sim 7,200 \text{ km s}^{-1}$) Pa α emission in the LIG F11058–1131, therefore confirming the discovery of a hidden BLR in this object from optical spectropolarimetry (Young et al. 1993). In addition, many of our objects present blue asymmetric wings at Pa α which can be attributed to faint broad-line emission with $\Delta V_{\text{FWHM}} \approx 2,000\text{--}4,000 \text{ km s}^{-1}$. However, in most cases (with the possible exceptions of F04103–2838, F13443+0802 SW, F14394+5332, and F16156+0146; see A4, A28, A33, and A35, respectively), this excess emission on the blue-shifted side of Pa α is probably associated with faint H₂ emission from the 7–5 O(3) λ 1.8721 and 6–4 O(5) λ 1.8665 transitions. As discussed in Black & van Dishoeck (1987) and VSK, each of these lines is expected to be about 1/3–1/4 the strength of the 1–0 S(3) transition if H₂ is excited through fluorescence (Black & van Dishoeck 1987). Combining the current sample with that of VSK, we therefore find seven ULIGs with obvious obscured BLRs. All seven of these objects are optically classified as Seyfert 2 galaxies, and all but one object (F23499+2423) are ‘warm’ galaxies with $f_{25}/f_{60} > 0.2$ (the LIG F11058–1131 also is a Seyfert 2 galaxy with warm colors).

As in VSK, the resolution of our spectra is insufficient to deblend the H₂ line at 1.958 μm from any possible [Si VI] λ 1.962 emission. Once again, we have to rely on the fact that fluorescent excitation of molecular hydrogen at low density predicts an H₂ 1–0 S(3)/1–0 S(1) flux ratio less than unity (typically ~ 0.7 ; Black & van Dishoeck 1987), while collisional excitation predicts a

ratio that ranges from 0.5 to 1.4 (Shull & Hollenbach 1978; Black & van Dishoeck 1987; Sternberg & Dalgarno 1989). We conservatively assume that [Si VI] λ 1.962 is present in galaxies where we measure what appears to be H₂ 1–0 S(3)/1–0 S(1) flux ratios larger than 1.4. As pointed out by VSK, this lower limit is confirmed in active galaxies with measured H₂ λ 1.958 and λ 2.122 line fluxes (e.g., Marconi et al. 1994). Only one object in the new sample clearly falls in this category: the Seyfert 2 galaxy F13305–1739, one of the two ULIGs in the new sample with broad Pa α . Two other Seyfert 2 galaxies, Mrk 273 and F13454–2956, may also present [Si VI] emission, but the evidence is less convincing. The H₂ 1–0 S(3) line intensity of the LINERs F04103–2838 and F08572+3915NW appears significantly larger than that of H₂ 1–0 S(1) but the H₂ λ 1.958 feature is partially blended with Br δ in both objects, making the intensity of this H₂ line uncertain. If it is assumed that the H₂ 1–0 S(3)/1–0 S(1) flux ratio in ULIGs is of order unity—as generally seems to be the case in optically selected Seyfert 2s (Marconi et al. 1994)—the [Si VI] λ 1.962 luminosities of F13305–1739, Mrk 273, and F13454–2956 are: 15, 0.8, and $2.0 \times 10^7 L_{\odot}$ (these luminosities have been corrected for reddening using the color excesses derived from the Pa α /H α ratios listed in Table 3). F13305–1739 is therefore more luminous than F12072–0444, the most powerful [Si VI] emitter previously known (cf. VSK and Ward et al. 1991).

4. Discussion

Our new data confirm the tendency reported by VSK for the warmer Seyfert 2 galaxies in the 1-Jy sample to reveal obscured BLRs at near-infrared wavelengths. All five objects in the combined sample of ULIGs with $f_{25}/f_{60} > 0.33$ (Pks 13451+1232, F13305–1739, Mrk 463E, F20460+1925, and F23060+0505) present obvious broad Paschen emission lines (note that the LIG F11058–1131 would also fall in this category). F05189–2524, another ULIG with unambiguous broad Pa α , is only marginally cooler than these objects ($f_{25}/f_{60} = 0.25$). The only other object in our sample with convincing broad Pa α , F23499+2423, has $f_{25}/f_{60} = 0.12$. This BLR detection rate among Seyfert 2 ULIGs appears to be higher than that found by Veilleux et al. (1997a) among optically-selected Seyfert 2s. However, it is important to mention that the results on the (low-redshift) optical Seyfert 2s relied on the detection of a broad-line component to the weak Pa β line rather than Pa α . Consequently, one cannot directly compare the results from these two studies.

Our combined dataset allows us to make stronger statements on the frequency of occurrence of nuclear activity among Seyfert 2 galaxies. Of the 22 ULIGs in the combined sample with optical Seyfert 2 spectra, 10 of them show either obvious broad Pa α or Pa β emission, or strong evidence for [Si VI] λ 1.962 emission. They are F05189–2524, F12072–0444, F13305–1739, Mrk 273, Pks 1345+12, F13454–2956, Mrk 463E, F20460+1925, F23060+0505, and F23499+2423 (recall that F11058–1131 is a LIG not a ULIG). Six additional Seyfert 2s from the combined sample may fall in this category (F08559+1053, F13443+0802 SW, F14394+5332, F16156+0146, F17179+5444, and F23233+2817), but data of higher spectral resolution are needed to confirm the presence of [Si VI]

emission in these objects or to determine the origin of the broad asymmetric wings to their Pa α profiles. Near-infrared signs of nuclear activity are therefore detected in 50 – 70% of the Seyfert 2 galaxies of the combined sample. These percentages are somewhat lower than those found by VSK. The slight difference is probably due to the larger fraction of ‘cool’ ULIGs in the combined sample. The combined sample constitutes a more representative subset of the whole (non-Seyfert 1) 1-Jy sample in terms of *IRAS* colors than the original sample of VSK. The results derived from the combined surveys should therefore be used when generalizing to the entire 1-Jy sample

Our near-infrared results suggest that at least half of the optically classified Seyfert 2 galaxies in the 1-Jy sample are genuine AGN. This is a lower limit to the actual number since our near-infrared method of AGN detection requires either the presence of a BLR or sufficient ionizing radiation with energies above 164 eV to produce detectable [Si VI] λ 1.962 emission. Some of the known optically selected Seyfert 2 galaxies do not present this feature (cf. Marconi et al. 1994). Note that the BLR detection rate among Seyfert 2 galaxies appears to be lower than the 100% (5 out of 5 or 6 out of 6 if the LIG F11058–1131 is also considered) detection rate among objects with $f_{25}/f_{60} > 1/3$. This stringent *IRAS* 25-to-60 μ m color criterion is therefore a better indicator of BLR activity in ULIGs than the Seyfert 2 characteristics at optical wavelengths.

The high BLR detection rate among ‘warm’ ULIGs suggests that the screen of dust in these objects is often optically thin at 2 μ m. Following VSK, we have plotted in Figure 3 the reddening-corrected Pa α luminosities of our sample galaxies as a function of their infrared luminosities. The reddening correction was carried out using the narrow-line extinctions listed in Table 3 and the lower limits on the broad-line extinctions derived in the Appendix. The solid line represents the relation found by Goldader et al. (1997a, 1997b) among lower luminosity infrared galaxies assuming a Pa α /Br γ ratio of 12 (case B recombination). A significant fraction of the data points fall below the solid line, therefore suggesting a deficit in Pa α emission in many ULIGs. This result is different from that of VSK, but is qualitatively similar to that of Goldader et al. (1995), who suggested that this deficit is an indication that dust obscuration is still important at 2 μ m in some of these objects. This apparent discrepancy with VSK is once again due to the larger percentage of ‘cool’ ULIGs in the combined sample. Figure 4 illustrates this point. The reddening-corrected Pa α -to-IR luminosity ratios of our sample galaxies are plotted as a function of their *IRAS* f_{25}/f_{60} ratio. As first pointed out by VSK, there is a clear tendency for the ‘warm’ ULIGs to present larger Pa α -to-IR luminosity ratios than ‘cool’ ULIGs. Note that this tendency is only visible when the Pa α fluxes include the contribution from the broad-line component.

Our new results therefore confirm that the *IRAS* f_{25}/f_{60} ratio is the primary factor determining the Pa α -to-IR luminosity ratio and the near-infrared detectability of obscured BLRs in ULIGs. ‘Warm’ ULIGs present optical and infrared properties which are intermediate between those of ‘cool’ ULIGs and optically selected quasars. But are the putative ‘buried quasars’ detected in these objects powerful enough to provide the bulk of the energy output? This question was first addressed by VSK using a sample of five objects with obscured BLRs. VSK expanded this analysis by including ten luminous and ultraluminous infrared galaxies with optically detected

BLRs (Seyfert 1s). Here, we further extend the analysis to include the data from the three buried quasars/AGN detected in the new sample (F05189–2524, F13305–1739, and the LIG F11058–131).

The results from this new analysis are presented in Figure 5, where the dereddened emission-line luminosities of the optical and obscured BLRs in infrared galaxies and in optically selected quasars are plotted as a function of bolometric luminosity. A discussion of the methods and assumptions which were used to create this figure is presented in VKS and summarized in the caption to Figure 5. The typical uncertainties on the data points of Figure 5 are of order $\pm 30\%$. The solid line in the figure is the best log-linear fit through the data of the optical quasars. To first order, this line therefore represents the relation found for pure broad-line AGNs⁷. Starburst-dominated ULIGs are expected to fall below this line. Figure 5 shows that F05189–2524 falls very close to the correlation derived for optical quasars, while F11058–1131 and F13305–1739 lie less than 0.5 dex below the correlation. Our new results thus provide further support to the idea first suggested by VSK and VKS that most ($\sim 80\%$) of the ULIGs with optical or near-infrared BLRs in the 1-Jy sample are powered predominantly by the quasar rather than by a powerful starburst. In other words, *the detection of an optical or near-infrared BLR in a ULIG (about 20% of the total 1-Jy sample) appears to be an excellent sign that the AGN is the dominant energy source in that ULIG.*

The good agreement in Figure 5 between optical quasars/Seyfert 1s and Seyfert 2s with obscured BLRs is not expected within the standard unification model of Seyfert galaxies. In this model, Seyfert 1s and 2s are fundamentally the same kind of objects and the viewing angle is the only parameter of importance in determining their appearance (cf., e.g., Antonucci 1993). Consequently, Seyfert 1s and 2s are expected to look the same when isotropic properties are compared. One such property is the far-infrared luminosity (since the far-infrared emission is usually assumed to be optically thin thermal emission; cf., e.g., Mulchaey et al. 1994 for a discussion of this issue). Another isotropic property is the luminosity of the BLR *after* correction for the extinction. The unification model therefore predicts that quasars/Seyfert 1s and Seyfert 2s should follow the same relation between the far-infrared luminosity and the extinction-corrected broad-line $H\beta$ luminosity. The agreement should break down when the bolometric luminosity is considered because the near-infrared, big-blue bump, and X-ray emission that contributes significantly to the bolometric luminosity of quasars/Seyfert 1s (but not to that of Seyfert 2s) is supposedly radiated anisotropically. This is not what we observe in Figure 5. Given that $L_{\text{IR}} \approx L_{\text{BOL}}$ in ULIGs and $L_{\text{IR}} \ll L_{\text{BOL}}$ in quasars, Figure 5 implies that the BLRs of obscured Seyfert 1 ULIGs are *underluminous* for a given far-infrared luminosity compared to the quasars. Within the context of the unification model, one could then interpret Figure 5 as evidence that the ULIGs produce a lot more far-infrared emission than “genuine” AGN with the same broad-line luminosity,

⁷Note, however, that even quasars may not be “pure AGN” since part of the far-infrared/submm emission may be produced by a dusty starburst (Rowan-Robinson 1995). Here, we assume that all of the far-infrared/submm emission is powered by the central AGN (Sanders et al. 1989). The far-infrared/submm emission generally contributes about 20% of the total bolometric luminosity of optical quasars.

thus that the AGN does *not* dominate their energetics.

Alternatively, the standard unification model may not apply to ULIGs. VKS have already pointed out that the standard unification model has difficulties explaining the larger percentage of Seyfert 1s relative to Seyfert 2s among ULIGs of higher infrared luminosities. It may be that the obscuring mass distribution in ULIGs varies with the luminosity of the energy source and with the optical spectral type. For instance, the trends with infrared luminosities can be explained if the covering factor decreases with increasing infrared luminosities (VKS). On the other hand, Figure 5 may indicate that Seyfert 2 ULIGs have much larger dust covering factors (and therefore reradiate a larger fraction of their bolometric luminosity in the far infrared) than optical quasars and Seyfert 1 ULIGs. Perhaps the obscuring material in Seyfert 2s has somehow had less time to settle into a disk than the material in optical quasars/Seyfert 1s.

A recent comparison of our optical/near-infrared results with those obtained with *ISO* (Lutz, Veilleux, & Genzel 1999) lends support to the scenario in which ULIGs with optical or obscured BLRs are powered predominantly by an AGN. Lutz et al. (1999) conclude that quasars constitute the dominant energy source in nearly all (10 out of the 11) optically classified Seyfert ULIGs in common between the *ISO* and optical samples. Strong AGN activity, once triggered, appears to quickly break the obscuring screen at least in certain directions, thus becoming detectable over a wide wavelength range.

The situation in LINERs and H II galaxies is more ambiguous. These objects represent about 70% of the entire 1-Jy sample (VKS). None of the 41 optically classified LINERs and H II galaxies in our near-infrared sample show any obvious signs of an obscured BLR or strong [Si VI] emission⁸. This apparent lack of an energetic AGN in these objects is consistent with the recent *ISO* results (Genzel et al. 1998; Lutz et 1999). As discussed by VSK, two possible scenarios can explain the near-infrared results on the LINERs and H II galaxies: (1) the cores of these ULIGs do not contain any AGN, (2) the optical depth due to dust is large enough to hide the AGN even at 2 μ m. The broad range of *IRAS* colors and Pa α -to-IR luminosity ratios among LINERs and H II galaxies (cf. Fig. 4) suggests that these objects are affected by dust screens of various optical depths. Dust obscuration is therefore unlikely to be the *only* reason why these objects present no obvious signs of AGN activity.

5. Conclusions

A sensitive near-infrared search for obscured broad-line regions was carried out in a set of thirty-nine ULIGs selected from the *IRAS* 1-Jy survey of 118 ULIGs (Kim & Sanders 1998). The

⁸Broad Pa α may be present in the LINER F04103–2838 (cf. A4), but spectra of higher spectral resolution are needed to confirm this result. [Si VI] λ 1.962 emission may also be present in this object and the LINER F08572+3915 NW, but contamination by Br δ makes the intensity of this feature uncertain.

results of this survey were combined with those obtained by VSK to produce a near-infrared spectroscopic database on sixty-four ULIGs. Prior to selecting these objects, the $\sim 10\%$ of the 118 galaxies that already were known optically to show direct signs of quasar activity, i.e. optically classified as Seyfert 1, were excluded. The sixty-four objects in the combined sample constitute a representative subset of the whole (non-Seyfert 1) 1-Jy sample, in terms of redshift, infrared luminosity, and *IRAS* colors. The results from the present survey can therefore be generalized with a high degree of confidence to the entire 1-Jy sample. These results can be summarized as follows:

1. Broad infrared recombination lines are detected in seven objects (all optically classified Seyfert 2s): F05198–2525, F13305–1739, Pks 1345+12 (= F13451+1232), Mrk 463E (= F13536+1836), F20460+1925, F23060+0505, and F23499+2423. Excess broad emission is also detected at the base of the Pa α profile in seven objects (all but one are optically classified Seyfert 2s): F04103–2838 (the only LINER), F08559+1053, F13443+0802 SW, F14394+5332, F16156+0146, F17179+5444, and F23233+2817. But new data are required to determine whether this emission is from H₂ $\lambda\lambda$ 1.8665, 1.8721 rather than from a genuine BLR. In addition, we confirm the spectropolarimetric discovery of a hidden BLR in the optically classified Seyfert 2 LIG F11058–1131.
2. The [Si VI] feature appears to be present in three additional objects (all optically classified Seyfert 2 galaxies), F12072–0444, Mrk 273 (= F13428+5608), and F13454–2956, and three or quite possibly four of the objects mentioned above: F13305–1739, Pks 1345+12, and F23233+2817, and perhaps F17179+5444. If these findings are confirmed by high-resolution spectroscopy, several of these objects would be among the most luminous [Si VI] emitters presently known ($\gtrsim 6 \times 10^7 L_{\odot}$).
3. From results 1 and 2 above, we find that all nine ‘warm’ ($f_{25}/f_{60} > 0.2$) optically classified Seyfert 2 galaxies in our sample of ULIGs show either obscured BLRs or [Si VI] emission at near-infrared wavelengths. None of these objects presents deficient Pa α -to-infrared luminosity ratios. These results support those derived from the smaller sample of VSK, and suggest that the screen of dust obscuring the cores of most ‘warm’ Seyfert 2 ULIGs is optically thin at 2 μ m.
4. No obvious signs of an obscured BLR or strong [Si VI] emission are detected in any of the 41 optically classified LINERs and H II galaxies in our sample. This result is consistent with recent mid-infrared *ISO* observations of ULIGs. The LINERs and H II galaxies in our sample span a wide range of *IRAS* colors and Pa α -to-IR luminosity ratios. The apparent lack of AGN activity in these objects is unlikely to be due solely to dust obscuration.

Recent results from an optical spectroscopic survey of the entire 1-Jy sample of 118 ULIGs (VKS) indicate that about 10% of these objects are optically classified as Seyfert 1s, while about

20% are optically classified as Seyfert 2s. Above $L_{\text{ir}} = 10^{12.3} L_{\odot}$, the Seyfert 1s and 2s represent $\sim 26\%$ and 23% of the ULIG population, respectively. Our near-infrared study of a representative subset of 64 of these ULIGs indicates that *at least* 50 – 70% (10 or possibly 16 out of 22) of the Seyfert 2s show signs of AGN activity at rest wavelenths shortward of $\sim 2 \mu\text{m}$ (BLR or [Si VI] emission). The optical and near-infrared data taken together, therefore suggest that the total fraction of objects in the 1-Jy sample with signs of a bonafide AGN is *at least* $\sim 20 - 25\%$. This fraction reaches 35 – 50% for objects with $L_{\text{ir}} > 10^{12.3} L_{\odot}$. These percentages are lower limits because the near-infrared method often fails to detect AGN activity ([Si VI] emission) in known optically selected Seyfert 2 galaxies (Marconi et al. 1994).

Comparisons of the dereddened emission-line luminosities of the optical or obscured BLRs detected in the ULIGs of the 1-Jy sample with those of optical quasars suggest that the AGN/quasar is the main source of energy in $\sim 80\%$ of all ULIGs with optical or near-infrared BLR. *At least* 15 – 25% of all ULIGs in the 1-Jy sample are therefore powered primarily by the AGN/quasar rather than by a starburst. This fraction is closer to 30 – 50% among ULIGs with $L_{\text{ir}} > 10^{12.3} L_{\odot}$. ULIGs with powerful AGN/quasar but with no or highly obscured BLRs would increase these percentages. These results are consistent with those derived from *ISO* data.

S. V. and D. B. S. thank the organizers of the 1998 Ringberg meeting where some of the issues in this paper were discussed, and the referee, Tim Heckman, for his comments on the standard unification model of Seyfert galaxies which helped improve this paper. This research was supported in part by JPL contract no. 961566 to the University of Hawaii (D. B. S.). S. V. gratefully acknowledges the financial support of NASA through LTSA grant NAG 56547 and Hubble fellowship HF-1039.01-92A awarded by the Space Telescope Science Institute which is operated by the AURA, Inc. for NASA under contract No. NAS5-26555. This research has made use of the NASA/IPAC Extragalactic Database (NED) which is operated by the Jet Propulsion Laboratory, California Institute of Technology, under contract with NASA.

APPENDIX

Notes on Individual Objects

In this Appendix the emission-line properties of each object are discussed, with particular emphasis on the presence or absence of broad components in the profiles of the infrared hydrogen recombination lines. In the cases where no positive detection of broad emission is reported, very conservative upper limits to the broad-line fluxes are given. These broad-line fluxes were determined by fitting the maximum broad Gaussian consistent with the data.

A1. IRAS F00188–0856

An upper limit of $F(\text{Pa}\alpha_{\text{bl}}) < 0.6 \times 10^{-14}$ ergs s⁻¹ cm⁻², assuming $\Delta V_{\text{FWHM}} \approx 7,000$ km s⁻¹, is derived in this optically classified LINER.

A2. IRAS F03250+1606

An upper limit of $F(\text{Pa}\alpha_{\text{bl}}) < 1 \times 10^{-14}$ ergs s⁻¹ cm⁻², assuming $\Delta V_{\text{FWHM}} \approx 6,400$ km s⁻¹, is derived in this optically classified LINER.

A3. IRAS F04074–2801

A wing is seen extending blueward from the base of Pa α in this optically classified LINER. A conservative fit to this wing emission gives $F(\text{Pa}\alpha_{\text{bl}}) \approx 0.5 \times 10^{-14}$ ergs s⁻¹ cm⁻² with $\Delta V_{\text{FWHM}} \approx 7,800$ km s⁻¹. However, contamination from H₂ $\lambda\lambda 1.8665, 1.8721$ may be responsible for this feature.

A4. IRAS F04103–2838

The optical spectrum of this object is ambiguous, spanning the boundary between H II galaxies and LINERs (VKS). Interestingly, this galaxy has the largest f_{25}/f_{60} among all of the LINERs and H II galaxies of our combined sample ($f_{25}/f_{60} = 0.30$). No obvious broad Pa α emission is visible in the infrared spectrum of this galaxy, but the Pa α profile presents a clear blue wing. A conservative fit to this wing emission gives $F(\text{Pa}\alpha_{\text{bl}}) \approx 1.5 \times 10^{-14}$ ergs s⁻¹ cm⁻² with $\Delta V_{\text{FWHM}} \approx 3,700$ km s⁻¹. Contamination from H₂ $\lambda\lambda 1.8665, 1.8721$ appears unlikely in this object considering the weaknesses of the other H₂ lines. The feature near 1.96 μm is considerably stronger than H₂ $\lambda 2.122$, suggesting that [Si VI] $\lambda 1.962$ may be present in this LINER. However, contamination from Br δ makes this statement uncertain.

A5. IRAS F04313–1649

This is the most distant source of our sample. There is no high-resolution optical spectrum of this object that could be used to determine the optical spectral type. This galaxy is relatively

faint at near-infrared wavelengths. No obvious broad Pa α emission is detected in this object. An upper limit of $F(\text{Pa}\alpha_{\text{bl}}) < 0.2 \times 10^{-14}$ ergs s $^{-1}$ cm $^{-2}$, assuming $\Delta V_{\text{FWHM}} \approx 2,300$ km s $^{-1}$, is derived.

A6. IRAS F05024–1941

The optical spectrum of this object is that of a Seyfert 2 galaxy (VKS), but it has relatively ‘cool’ *IRAS* 25-to-60 μm color ($f_{25}/f_{60} = 0.13$). This object is faint at near-infrared wavelengths. No obvious broad Pa α emission is detected in this object within the uncertainties of our data. An upper limit of $F(\text{Pa}\alpha_{\text{bl}}) < 0.3 \times 10^{-14}$ ergs s $^{-1}$ cm $^{-2}$, assuming $\Delta V_{\text{FWHM}} \approx 2,500$ km s $^{-1}$, is derived.

A7. IRAS F05156–3024

The optical spectrum of this object is that of a Seyfert 2 galaxy (VKS), but it presents ‘cool’ *IRAS* 25-to-60 μm color ($f_{25}/f_{60} = 0.089$). A weak wing is seen extending blueward from the base of Pa α in this object. A conservative fit to this wing emission gives $F(\text{Pa}\alpha_{\text{bl}}) \approx 0.5 \times 10^{-14}$ ergs s $^{-1}$ cm $^{-2}$ with $\Delta V_{\text{FWHM}} \approx 2,400$ km s $^{-1}$. However, contamination from H $_2$ $\lambda\lambda 1.8665, 1.8721$ may be responsible for this feature.

A8. IRAS F05189–2524

This object is one of six ULIGs from the BGS sample of Sanders et al. (1988a) included in the present study. This is the warmest object of this set ($f_{25}/f_{60} = 0.25$). The optical spectrum of this object is that of a Seyfert 2 galaxy (Veilleux et al. 1995). The K-band spectrum of this object clearly shows the presence of broad ($\Delta V_{\text{FWHM}} \approx 2,600$ km s $^{-1}$) emission at Pa α . This spectrum also illustrates very well the difficulty in detecting the broad component to Br γ . This explains the negative results of Goldader et al. (1995) on this object. The J-band spectrum confirms the presence of broad emission in the recombination lines. Both Pa β and He I $\lambda 1.0832$ present broad profiles. Note, however, that the broad line parameters derived from the J-band spectrum are considered less accurate than those derived from Pa α because both Pa β and He I $\lambda 1.0832$ are weaker than Pa α , and the intensities and profiles of both lines are affected by strong atmospheric absorption features. Based on the broad Pa α flux listed in Table 3 and the assumption that a BLR with one-third the intensity of the observed H α emission would have been detected in the optical spectrum of VKS, a lower limit to the color excess in the BLR of $E(B - V)_{\text{bl}} > 2.8$ mag is derived.

A9. IRAS F08201+2801

An upper limit of $F(\text{Pa}\alpha_{\text{bl}}) < 0.2 \times 10^{-14}$ ergs s $^{-1}$ cm $^{-2}$, assuming $\Delta V_{\text{FWHM}} \approx 6,600$ km s $^{-1}$, is derived in this optically classified H II galaxy.

A10. IRAS F08572+3915 NW

This object is part of the original set of 10 ULIGs from the BGS sample (Sanders et al. 1988a). The optical spectrum of this relatively ‘warm’ object ($f_{25}/f_{60} = 0.23$) is ambiguous, spanning the boundary between H II galaxies and LINERs (Veilleux et al. 1995; VKS). Our near-infrared spectrum does not reveal any obvious signs of an obscured AGN (BLR or [Si VI] feature) at near-infrared wavelengths. An upper limit of $F(\text{Pa}\alpha_{\text{bl}}) < 1 \times 10^{-14}$ ergs s⁻¹ cm⁻², assuming $\Delta V_{\text{FWHM}} \approx 6,700$ km s⁻¹, is derived. A comparison of the H₂ $\lambda 1.958$ and $\lambda 2.122$ fluxes suggests the presence of [Si VI] $\lambda 1.962$ emission in this galaxy, but this conclusion is very uncertain because H₂ $\lambda 1.958$ is clearly blended with Br δ .

A11. IRAS F10091+4704

This powerful LINER/H II galaxy presents very strong H₂ 1–0 S(3) $\lambda 1.958$ and 1–0 S(5) $\lambda 1.835$ lines relative to Pa α . Weak [Fe II] $\lambda 1.644$ is also detected in this object. The relatively poor signal-to-noise ratio of the spectrum near Pa α (in part due to corrections for atmospheric absorption features at those wavelengths) prevents us from making a strong statement on the presence of a BLR in this object. An upper limit of $F(\text{Pa}\alpha_{\text{bl}}) < 0.1 \times 10^{-14}$ ergs s⁻¹ cm⁻², assuming $\Delta V_{\text{FWHM}} \approx 5,800$ km s⁻¹, is derived. We cannot make any statement on the existence of [Si VI] $\lambda 1.962$ in this object because the critical H₂ line at 2.122 μm is not included within the spectral range of our spectrum.

A12. IRAS F10190+1322

This low-redshift H II galaxy shows no obvious signs of obscured BLRs or [Si VI] $\lambda 1.962$ emission. An upper limit of $F(\text{Pa}\alpha_{\text{bl}}) < 0.3 \times 10^{-14}$ ergs s⁻¹ cm⁻², assuming $\Delta V_{\text{FWHM}} \approx 7,300$ km s⁻¹, is derived.

A13. IRAS F10594+3818

This object is optically classified as an H II galaxy (VKS). It shows no obvious signs of obscured BLRs or [Si VI] $\lambda 1.962$ emission. An upper limit of $F(\text{Pa}\alpha_{\text{bl}}) < 0.6 \times 10^{-14}$ ergs s⁻¹ cm⁻², assuming $\Delta V_{\text{FWHM}} \approx 7,300$ km s⁻¹, is derived.

A14. IRAS F11028+3130

Our near-infrared spectrum of this LINER is essentially featureless. An upper limit on the total Pa α flux of $F(\text{Pa}\alpha) < 0.04 \times 10^{-14}$ ergs s⁻¹ cm⁻², assuming $\Delta V_{\text{FWHM}} \approx 500$ km s⁻¹, is derived.

A15. IRAS F11095–0237

The optical spectrum of this object is that of a LINER. Our infrared spectrum does not show any evidence for broad Pa α or [Si VI] $\lambda 1.962$ emission. An upper limit of $F(\text{Pa}\alpha_{\text{bl}}) < 0.6 \times 10^{-14}$ ergs s⁻¹ cm⁻², assuming $\Delta V_{\text{FWHM}} \approx 6,500$ km s⁻¹, is derived.

A16. IRAS F11180+1623

There is no obvious signs of broad emission in the Pa α profile of this LINER/H II galaxy. An upper limit of $F(\text{Pa}\alpha_{\text{bl}}) < 0.2 \times 10^{-14}$ ergs s $^{-1}$ cm $^{-2}$, assuming $\Delta V_{\text{FWHM}} \approx 6,500$ km s $^{-1}$, is derived. We cannot make any strong statement on the existence of [Si VI] $\lambda 1.962$ in this object because the H $_2$ $\lambda 2.122$ feature is close to the edge of the spectrum and is strongly affected by atmospheric absorption features.

A17. IRAS F11223–1244

There is no obvious signs for broad Pa α emission in this ‘cool’ ($f_{25}/f_{60} = 0.11$) Seyfert 2 galaxy. An upper limit of $F(\text{Pa}\alpha_{\text{bl}}) < 0.4 \times 10^{-14}$ ergs s $^{-1}$ cm $^{-2}$, assuming $\Delta V_{\text{FWHM}} \approx 7,500$ km s $^{-1}$, is derived. We cannot make any strong statement on the existence of [Si VI] $\lambda 1.962$ in this galaxy because our spectrum does not extend longward enough in wavelength to include the critical H $_2$ $\lambda 2.122$ line. An upper limit to the broad Pa α flux of $F(\text{Pa}\alpha_{\text{bl}}) < 0.3 \times 10^{-14}$ erg s $^{-1}$ cm $^{-2}$, assuming $\Delta V_{\text{FWHM}} \approx 5,000$ km s $^{-1}$, is derived.

A18. IRAS F11506+1331

The optical spectrum of this object is ambiguous, spanning the boundary between H II galaxies and LINERs (VKS). The near-infrared spectrum is dominated by the strong Pa α feature. The relatively weak H $_2$ lines are typical of those observed in optically classified H II galaxies (cf. Fig. 1). There is no obvious signs of AGN activity in this galaxy (BLR or [Si VI] $\lambda 1.962$ feature). An upper limit of $F(\text{Pa}\alpha_{\text{bl}}) < 1 \times 10^{-14}$ ergs s $^{-1}$ cm $^{-2}$, assuming $\Delta V_{\text{FWHM}} \approx 6,300$ km s $^{-1}$, is derived.

A19. IRAS F11582+3020

No broad Pa α emission is detected in this LINER within the uncertainties of our measurements. An upper limit of $F(\text{Pa}\alpha_{\text{bl}}) < 0.2 \times 10^{-14}$ ergs s $^{-1}$ cm $^{-2}$, assuming $\Delta V_{\text{FWHM}} \approx 3,600$ km s $^{-1}$, is derived. The spectral range of our spectrum prevents us from measuring the strength of H $_2$ $\lambda 2.122$ and comparing it with that of H $_2$ $\lambda 1.958$. The feature at $1.96 \mu\text{m}$ is also too faint for detailed profile analysis. Therefore, no statement can be made on the existence of [Si VI] $\lambda 1.962$ in this galaxy.

A20. IRAS F12018+1941

The optical spectral type of this galaxy (LINER) was derived using the measurements of Armus et al. (1989). There is no evidence for [Si VI] $\lambda 1.962$ or broad Pa α emission in this object. The continuum near Pa α appears slightly convex, but this may be due to contaminants redward of Pa α . A very conservative upper limit to the broad Pa α flux in this galaxy was derived by assuming that the convexity in the continuum is due entirely to broad Pa α emission: $F(\text{Pa}\alpha_{\text{bl}}) < 0.5 \times 10^{-14}$ ergs s $^{-1}$ cm $^{-2}$, assuming $\Delta V_{\text{FWHM}} \approx 8,300$ km s $^{-1}$.

A21. IRAS F12032+1707

This object shares many resemblances with F10091+4704 (cf. A11). Both of these galaxies are powerful ($\log[L_{\text{IR}}/L_{\odot}] > 12.5$) ULIGs with LINER characteristics at optical wavelengths and with strong H_2 emission lines relative to $\text{Pa}\alpha$. The [Fe II] $\lambda 1.644$ feature is also detected in both galaxies, and none of these objects show any obvious signs for broad $\text{Pa}\alpha$. The quality of our spectrum of F12032+1707 is slightly better than that of F10091+4704, therefore allowing us to derive a strong upper limit to the flux from broad $\text{Pa}\alpha$: $F(\text{Pa}\alpha_{\text{bl}}) < 0.6 \times 10^{-14}$ ergs $\text{s}^{-1} \text{cm}^{-2}$, assuming $\Delta V_{\text{FWHM}} \approx 7,800 \text{ km s}^{-1}$. No statement can be made about the presence of [Si VI] $\lambda 1.962$ in this object because the H_2 $\lambda 2.122$ is redshifted out of our spectral range.

A22. IRAS F12112+0305

The optical spectrum of this BGS ULIG shows the signatures of a LINER. The relatively low redshift of this object shifts the $\text{Pa}\alpha$ line into a region of the spectrum which is affected by atmospheric absorption features. Nevertheless, the excellent correction for these features (as evident from the flat and featureless continuum in this region) allows us to derive a strong upper limit to the flux from broad $\text{Pa}\alpha$: $F(\text{Pa}\alpha_{\text{bl}}) < 0.7 \times 10^{-14}$ ergs $\text{s}^{-1} \text{cm}^{-2}$ assuming $\Delta V_{\text{FWHM}} \approx 6,000 \text{ km s}^{-1}$. The H_2 lines in this object are all very faint relative to $\text{Pa}\alpha$.

A23. IRAS F12447+3721

The infrared spectrum of this H II galaxy is similar to that of F15206+3342, another H II galaxy in the sample of VSK: strong narrow emission from $\text{Pa}\alpha$ is visible superposed on a faint continuum; the lines from H_2 are barely or not detected. An upper limit to the broad $\text{Pa}\alpha$ flux of $F(\text{Pa}\alpha_{\text{bl}}) < 0.6 \times 10^{-14}$ erg $\text{s}^{-1} \text{cm}^{-2}$, assuming $\Delta V_{\text{FWHM}} \approx 2,700 \text{ km s}^{-1}$, is derived.

A24. IRAS F13106–0922

The optical spectrum of this object is ambiguous, spanning the boundary between H II galaxies and LINERs (VKS). No obvious signs of [Si VI] $\lambda 1.962$ or broad $\text{Pa}\alpha$ emission are detected in this object. An upper limit to the broad $\text{Pa}\alpha$ flux of $F(\text{Pa}\alpha_{\text{bl}}) < 0.3 \times 10^{-14}$ erg $\text{s}^{-1} \text{cm}^{-2}$, assuming $\Delta V_{\text{FWHM}} \approx 5,000 \text{ km s}^{-1}$, is derived.

A25. IRAS F13305–1739

The infrared spectrum of this ‘warm’ ($f_{25}/f_{60} = 0.34$) Seyfert 2 galaxy presents broad ($\Delta V_{\text{FWHM}} \approx 3,000 \text{ km s}^{-1}$) $\text{Pa}\alpha$ emission but very little H_2 emission. Based on the broad $\text{Pa}\alpha$ flux listed in Table 3 and the assumption that a BLR with one-third the intensity of the observed $\text{H}\alpha$ emission would have been detected in the optical spectrum of VKS, a lower limit to the color excess in the BLR of $E(B - V)_{\text{bl}} > 0.8$ mag is derived. Comparison of the H_2 $\lambda 1.958$ and $\lambda 2.122$ fluxes also suggests the presence of [Si VI] $\lambda 1.962$ emission in this galaxy.

A26. Mrk 273 = IRAS F13428+5608

This relatively ‘cool’ ($f_{25}/f_{60} = 0.10$) ULIG from the original BGS sample (Sanders et al. 1988a) show Seyfert 2 characteristics at optical wavelengths (Kim et al. 1998). Our J- and K-band spectra of this object show no clear evidence for broad emission. The continuum near Pa α appears slightly convex, but this may be due to our correction for atmospheric absorption in this spectral region. A very conservative upper limit to the broad Pa α flux in this galaxy was derived by assuming that the convexity in the continuum is due entirely to broad Pa α emission: $F(\text{Pa}\alpha_{\text{bl}}) < 3.7 \times 10^{-14} \text{ ergs s}^{-1} \text{ cm}^{-2}$, assuming $\Delta V_{\text{FWHM}} \approx 7,600 \text{ km s}^{-1}$. An upper limit to the broad Pa β and He I $\lambda 1.083$ fluxes was also derived from the J-band spectrum: $F(\text{He I}_{\text{bl}}) < 1.5 \times 10^{-14} \text{ ergs s}^{-1} \text{ cm}^{-2}$, assuming $\Delta V_{\text{FWHM}} \approx 7,500 \text{ km s}^{-1}$. Comparison of the H $_2$ $\lambda 1.958$ and $\lambda 2.122$ fluxes suggests the presence of [Si VI] $\lambda 1.962$ emission in this galaxy, but the evidence is marginal because the H $_2$ $\lambda 1.958/\text{H}_2$ $\lambda 2.122$ flux ratio is only ~ 1.4 and contamination from Br δ makes the flux of H $_2$ $\lambda 1.958$ uncertain.

A27. IRAS F13443+0802 NE

The infrared spectrum of this H II galaxy presents very weak H $_2$ emission lines and does not show any evidence for broad Pa α emission. An upper limit to the broad Pa α flux of $F(\text{Pa}\alpha_{\text{bl}}) < 0.5 \times 10^{-14} \text{ erg s}^{-1} \text{ cm}^{-2}$, assuming $\Delta V_{\text{FWHM}} \approx 4,800 \text{ km s}^{-1}$, is derived.

A28. IRAS F13443+0802 SW

This is the galaxy in our sample with the lowest apparent Pa α flux. Nevertheless, the S/N in the continuum is sufficient to put strong constraints on any broad component to Pa α . A weak blue wing is detected at the base of Pa α in this Seyfert. A Gaussian fit to this feature gives $F(\text{Pa}\alpha_{\text{bl}}) \approx 0.2 \times 10^{-14} \text{ erg s}^{-1} \text{ cm}^{-2}$ with a $\Delta V_{\text{FWHM}} \approx 2,400 \text{ km s}^{-1}$. Part of this feature may be attributed to H $_2$ $\lambda\lambda 1.8665, 1.8721$. The line profile of H $_2$ $\lambda 1.957$ appears unusually broad ($\Delta V_{\text{FWHM}} \approx 1,250 \text{ km s}^{-1}$), but it is uncertain. The signal-to-noise of our spectrum near H $_2$ $\lambda 2.122$ is rather poor and prevents us from making a strong statement on the relative intensity of H $_2$ $\lambda 1.958$ and H $_2$ $\lambda 2.122$.

A29. IRAS F13454–2956

This Seyfert 2 galaxy has an unusually ‘cool’ 25-to-60 μm IRAS flux ratio of only 0.03. There is no obvious signs of broad emission in the profile of Pa α . The excellent signal-to-noise ratio of our near-infrared spectrum allows us to put strong constraints on any broad component to Pa α : $F(\text{Pa}\alpha_{\text{bl}}) \approx 0.4 \times 10^{-14} \text{ erg s}^{-1} \text{ cm}^{-2}$, assuming a $\Delta V_{\text{FWHM}} \approx 6,600 \text{ km s}^{-1}$. Comparison of the H $_2$ $\lambda 1.958$ and $\lambda 2.122$ fluxes suggests the presence of [Si VI] $\lambda 1.962$ emission in this galaxy.

A30. IRAS F13509+0442

The near-infrared spectrum of this H II galaxy presents strong Pa α but weak H₂. No obvious broad Pa α emission is visible in our spectrum. An upper limit of $F(\text{Pa}\alpha_{\text{bl}}) < 0.8 \times 10^{-14}$ ergs s⁻¹ cm⁻², assuming $\Delta V_{\text{FWHM}} \approx 4,000$ km s⁻¹, is derived.

A31. IRAS F14053–1958

The only near-infrared emission line detected in this Seyfert 2 galaxy is narrow Pa α . An upper limit of $F(\text{Pa}\alpha_{\text{bl}}) < 0.2 \times 10^{-14}$ ergs s⁻¹ cm⁻², assuming $\Delta V_{\text{FWHM}} \approx 2,300$ km s⁻¹, is derived.

A32. IRAS F14070+0525

This object is the most powerful ULIG in our sample. The infrared spectrum of this Seyfert 2 galaxy is dominated by narrow Pa α . The [Fe II] $\lambda 1.644$ feature is also present at considerably fainter flux levels. An upper limit of $F(\text{Pa}\alpha_{\text{bl}}) < 0.2 \times 10^{-14}$ ergs s⁻¹ cm⁻², assuming $\Delta V_{\text{FWHM}} \approx 3,800$ km s⁻¹, is derived.

A33. IRAS F14394+5332

Several emission lines from H I and H₂ are detected in the near-infrared spectrum of this Seyfert 2 galaxy. A weak blue wing is detected at the base of Pa α . A Gaussian fit to this feature gives $F(\text{Pa}\alpha_{\text{bl}}) \approx 2 \times 10^{-14}$ erg s⁻¹ cm⁻² with a $\Delta V_{\text{FWHM}} \approx 6,300$ km s⁻¹. Part of this feature may be attributable to H₂ $\lambda\lambda 1.8665, 1.8721$. There is no evidence for strong [Si VI] emission in this object.

A34. IRAS F15250+3609

The optical spectrum of this BGS ULIG is ambiguous, straddling the boundary between H II galaxies and LINERs (VKS). There is no obvious signs for an obscured broad-line region or strong [Si VI] $\lambda 1.962$ emission in this galaxy. An upper limit of $F(\text{Pa}\alpha_{\text{bl}}) < 1.4 \times 10^{-14}$ ergs s⁻¹ cm⁻², assuming $\Delta V_{\text{FWHM}} \approx 5,500$ km s⁻¹, is derived.

A35. IRAS F16156+0146

A blue wing is detected at the base of Pa α in this optical Seyfert 2. A Gaussian fit to this feature gives $F(\text{Pa}\alpha_{\text{bl}}) \approx 0.7 \times 10^{-14}$ erg s⁻¹ cm⁻² with a $\Delta V_{\text{FWHM}} \approx 5,600$ km s⁻¹. Part of this feature may be attributable to H₂ $\lambda\lambda 1.8665, 1.8721$.

A36. IRAS F16300+1558

This optically classified LINER presents strong narrow Pa α and weak H₂ $\lambda 1.958$ and [Fe II] $\lambda 1.644$. An upper limit of $F(\text{Pa}\alpha_{\text{bl}}) < 0.3 \times 10^{-14}$ ergs s⁻¹ cm⁻², assuming $\Delta V_{\text{FWHM}} \approx 3,500$ km s⁻¹, is derived.

A37. IRAS F17208–0014

This BGS ULIG is optically classified as an H II galaxy (Veilleux et al. 1995). There is no obvious broad Pa α emission in this object within the uncertainties of the data. Errors in correcting for the presence of atmospheric absorption features near Pa α increases the noise in this region. A very conservative Gaussian fit of the emission under narrow Pa α gives $F(\text{Pa}\alpha_{\text{bl}}) \approx 2 \times 10^{-14} \text{ erg s}^{-1} \text{ cm}^{-2}$ with a $\Delta V_{\text{FWHM}} \approx 4,700 \text{ km s}^{-1}$.

A38. IRAS F22491–1808

This H II galaxy is part of the original BGS sample of ULIGs (Sanders et al. 1988). The near-infrared spectrum of this object presents only very weak H₂ emission and no evidence for strong [Si VI] or broad Pa α emission within the uncertainties of the data. Errors in correcting for the presence of atmospheric absorption features near Pa α increases the noise in this region. A very conservative Gaussian fit of the emission under narrow Pa α gives $F(\text{Pa}\alpha_{\text{bl}}) \approx 0.4 \times 10^{-14} \text{ erg s}^{-1} \text{ cm}^{-2}$ with a $\Delta V_{\text{FWHM}} \approx 6,400 \text{ km s}^{-1}$.

A39. IRAS F23365+3604

The infrared spectrum of this optical LINER shows no evidence for an obscured broad-line region or strong [Si VI] $\lambda 1.962$ emission. An upper limit of $F(\text{Pa}\alpha_{\text{bl}}) < 1 \times 10^{-14} \text{ ergs s}^{-1} \text{ cm}^{-2}$, assuming $\Delta V_{\text{FWHM}} \approx 3,300 \text{ km s}^{-1}$, is derived.

A40. IRAS F11058–1131 (LIG)

Optical spectropolarimetry of this luminous infrared galaxy by Young et al. (1993) reveals a hidden BLR, seen in scattered, polarized light. Young et al. measure $\Delta V_{\text{FWHM}} \approx 7,600 \text{ km s}^{-1}$ and $\Delta V_{\text{FWZI}} \approx 16,800 \text{ km s}^{-1}$ for polarized H α . The infrared spectrum of this Seyfert 2 galaxy is equally stunning: broad ($\Delta V_{\text{FWHM}} \approx 7,200 \text{ km s}^{-1}$) wings are clearly visible at Pa α , extending to $\sim \pm 10,000 \text{ km s}^{-1}$ at zero intensity and beautifully confirming the results of Young et al. (1993). The ratio of Pa α_{bl} emission to scattered H α_{bl} emission is ~ 8 , nearly two orders of magnitude larger than the value predicted from case B recombination. If we make the rather safe assumption that a BLR with one-third the intensity of the observed H α emission would have been detected in the optical spectrum of Osterbrock & de Robertis (1985), we derive a lower limit to the color excess towards the BLR based on Pa $\alpha_{\text{bl}}/\text{H}\alpha_{\text{nl}}$ of $E(B - V)_{\text{bl}} > 1.4$.

Table 1: Sample.

IRAS	z	$f_\nu(\lambda)$ (Jy)				FQ ^a	$\frac{f_{25}}{f_{60}}$ log	$\frac{f_{60}}{f_{100}}$ log	$\frac{L_{IR}}{L_\odot}$ log	Optical Sp. Type
		12 μ m	25 μ m	60 μ m	100 μ m					
F00188–0856	0.128	0.12	0.37	2.59	3.40	1332	–0.85	–0.12	12.33	L
F03250+1606	0.129	0.10	0.15	1.38	1.77	1132	–0.96	–0.11	12.06	L
F04074–2801	0.153	0.07	0.07	1.33	1.72	1a32	–1.28	–0.11	12.14	L
F04103–2838	0.118	0.08	0.54	1.82	1.71	2332	–0.53	+0.03	12.15	L:
F04313–1649	0.268	0.07	0.07	1.01	1.10	1232	–1.16	–0.04	12.55	...
F05024–1941	0.192	0.15	0.14	1.06	1.34	a232	–0.88	–0.10	12.43	S2
F05156–3024	0.171	0.08	0.10	1.16	1.40	1232	–1.06	–0.08	12.20	S2
F05189–2524	0.042	0.73	3.44	13.67	11.36	3332	–0.60	+0.08	12.07	S2
F08201+2801	0.168	0.09	0.15	1.17	1.43	1a32	–0.89	–0.09	12.23	H
F08572+3915 NW	0.058	0.32	1.70	7.43	4.59	3332	–0.64	+0.21	12.11	L:
F10091+4704	0.246	0.06	0.08	1.18	1.55	1132	–1.17	–0.12	12.67	L:
F10190+1322	0.077	0.07	0.38	3.33	5.57	1232	–0.94	–0.22	12.00	H
F10594+3818	0.158	0.09	0.15	1.29	1.89	1132	–0.93	–0.17	12.24	H
F11028+3130	0.199	0.09	0.09	1.02	1.44	1a32	–1.05	–0.15	12.32	L
F11095–0237	0.106	0.06	0.42	3.25	2.53	a332	–0.89	+0.11	12.20	L
F11180+1623	0.166	0.08	0.19	1.19	1.60	1132	–0.80	–0.13	12.24	L:
F11223–1244	0.199	0.07	0.16	1.52	2.26	1132	–0.98	–0.17	12.59	S2
F11506+1331	0.127	0.10	0.19	2.58	3.32	1a32	–1.13	–0.11	12.28	H:
F11582+3020	0.223	0.10	0.15	1.13	1.49	1132	–0.88	–0.12	12.56	L
F12018+1941	0.169	0.11	0.37	1.76	1.78	1232	–0.68	+0.00	12.44	L ^b
F12032+1707	0.217	0.14	0.25	1.36	1.54	1a32	–0.74	–0.05	12.57	L
F12112+0305	0.073	0.12	0.51	8.50	9.98	a332	–1.22	–0.07	12.28	L
F12447+3721	0.158	0.12	0.10	1.04	0.84	1a32	–0.94	+0.09	12.06	H
F13106–0922	0.174	0.12	0.06	1.24	1.89	1122	–1.32	–0.18	12.32	L:
F13305–1739	0.148	0.09	0.39	1.16	1.04	1232	–0.47	+0.05	12.21	S2
F13428+5608 ^b	0.037	0.24	2.28	21.74	21.38	3332	–0.98	+0.01	12.10	S2
F13443+0802 NE/SW	0.135	0.12	0.11	1.50	1.99	1132	–1.07	–0.12	12.15	H/S2
F13454–2956	0.129	0.06	0.07	2.16	3.38	1a32	–1.49	–0.19	12.21	S2
F13509+0442	0.136	0.10	0.23	1.56	2.53	2132	–0.83	–0.21	12.27	H
F14053–1958	0.161	0.07	0.14	1.02	1.12	1132	–0.86	–0.04	12.12	S2
F14070+0525	0.265	0.07	0.19	1.45	1.82	1a32	–0.88	–0.10	12.76	S2
F14394+5332	0.105	0.03	0.35	1.95	2.39	a332	–0.75	–0.09	12.04	S2
F15250+3609 ^d	0.055	0.20	1.32	7.29	5.91	1332	–0.74	+0.09	11.97	L:
F16156+0146	0.132	0.10	0.28	1.13	1.00	1332	–0.61	+0.05	12.04	S2
F16300+1558	0.242	0.07	0.07	1.48	1.99	1a32	–1.33	–0.13	12.63	L
F17208–0014 ^d	0.043	0.20	1.66	31.14	34.90	2332	–1.27	–0.05	12.39	H
F22491–1808	0.076	0.05	0.55	5.44	4.45	a232	–1.00	+0.09	12.09	H
F23365+3604 ^d	0.064	0.10	0.81	7.09	8.36	1332	–0.94	–0.07	12.10	L
F11058–1131 ^d (LIG)	0.055 ^e	0.15	0.32	0.77	0.79	1232	–0.38	–0.01	11.27	S2 ^e

^a Flux quality in each of the four *IRAS* bands. Numbers 1-3 are the quality flags adopted for the *IRAS* catalogs (1 = upper limit, 2 = moderate quality, 3 = high quality). The letter ‘a’ means that the flux density was estimated by Kim & Sanders (1998) after coadding all of the *IRAS* data available for the source using the ADDSCAN/SCANPI procedure (Helou et al. 1988); these ‘low quality’ measurements are typically 2-3 σ detections.

^b Based on the line ratios measured by Armus, Heckman, & Miley (1989). Only a lower limit is available on the [O III] λ 0.5007/H β ratio. It is therefore possible that this object is a Seyfert 2 galaxy instead of a LINER.

^c Other name: F13428+5608 = Mrk 273.

^d Infrared properties from the *IRAS* Faint Source Catalog, Version 2 (Moshir et al. 1992).

^e Redshift and optical spectral type from Osterbrock & de Robertis (1985).

Note. — Unless otherwise noted, infrared properties and optical spectral types are from Kim & Sanders (1998), Kim, Veilleux, & Sanders (1998), or Veilleux et al (1995, 1999).

Table 2: Journal of Observations.

IRAS (1)	Date (2)	Exp (min) (3)	Res ($\frac{\lambda}{\Delta\lambda}$) (4)
F00188–0856	1997 Dec 27	64	430
F03250+1606	1997 Dec 28	32	430
F04074–2801	1997 Dec 28	64	430
F04103–2838	1997 Dec 28	16	430
F04313–1649	1998 Mar 05	80	400
F05024–1941	1997 Dec 27	64	430
F05156–3024	1997 Dec 27	32	430
F05189–2524	1997 Dec 27	16	430
	1997 Dec 28	16	430
	1997 Dec 28	24	500
F08201+2801	1997 Dec 28	48	430
F08572+3915 NW	1997 Dec 27	40	430
F10091+4704	1997 Dec 27	80	430
F10190+1322	1998 Mar 04	64	400
F10594+3818	1998 Mar 04	32	400
F11028+3130	1998 Mar 05	64	400
F11095–0237	1998 Mar 04	48	400
F11180+1623	1998 Mar 04	48	400
F11223–1244	1997 Dec 27	64	430
F11506+1331	1998 Mar 04	16	400
F11582+3020	1997 Dec 28	64	430
F12018+1941	1998 Mar 04	32	400
F12032+1707	1998 Mar 05	32	400
F12112+0305	1997 Dec 27	32	430
	1997 Dec 28	32	430
F12447+3721	1998 Mar 07	24	400
F13106–0922	1998 Mar 05	64	400
F13305–1739	1998 Mar 04	32	400
F13428+5608	1998 Mar 04	16	400
	1998 Mar 07	16	460
F13443+0802 NE	1998 Mar 06	24	400
F13443+0802 SW	1998 Mar 06	48	400
F13454–2956	1998 Mar 06	48	400
F13509+0442	1998 Mar 04	24	400
F14053–1958	1998 Mar 06	40	400
	1998 Mar 07	32	400
F14070+0525	1998 Mar 04	32	400
	1998 Mar 06	48	400
F14394+5332	1998 Mar 05	16	400
F15250+3609	1998 Mar 05	16	400
F16156+0146	1998 Mar 05	48	400
F16300+1558	1998 Mar 07	40	400
F17208–0014	1998 Mar 05	16	400
F22491–1808	1997 Dec 28	48	430
F23365+3604	1997 Dec 28	32	430
F11058–1131 (LIG)	1998 Mar 05	16	400

Table 3: Optical^a and Near-Infrared Line Measurements.

IRAS		H β_{nl}	H α_{nl}	[Fe II]	H ₂	Pa α_{nl}	Pa α_{bl}	Br δ	H ₂ 1.958	H ₂	He I	H ₂	Br γ	H α /H β	Pa α /H β
(1)	(2)	(3)	(4)	1.644 (5)	1.835 (6)	1.875 (7)	1.875 (8)	1.945 (9)	+ [Si VI] 1.962 (10)	2.033 (11)	2.058 (12)	2.121 (13)	(14)	(15)	(16)
F00188-0856	<i>F</i>	0.0245	0.35	...	0.109	0.907	0.204	0.4:	0.2:	1.56	1.75
	<i>EW</i>			...	6.0	49	11.3	21:	12:		
	<i>W</i>			...	689:	831	875	1200::	1320::		
	<i>W_c</i>		0:	448	526	975::	1120::		
F03250+1606	<i>F</i>	0.0220	0.44	3.00	0.311	...	0.11:	0.20:	0.23:	1.93	2.25
	<i>EW</i>			126	15.2	...	5.9:	10.2:	12.4:		
	<i>W</i>			813	884:	...	570::	611::	804::		
	<i>W_c</i>		320:	414	539:	...	0::	0::	395::		
F04074-2801	<i>F</i>	0.0077	0.07	...	0.138	0.459	0.192	0.275	...	1.12	2.25
	<i>EW</i>			...	13.7	47.5	22.5	38.4	...		
	<i>W</i>			...	961:	803	788	882	...		
	<i>W_c</i>		658:	392	362	536	...		
F04103-2838	<i>F</i>	0.128	1.42	3.37	...	0.17:	0.393	0.14:	0.441	1.25	1.65
	<i>EW</i>			166	...	8.1:	19.5	7.1:	22.8		
	<i>W</i>			827	...	754::	1092:	447::	717:		
	<i>W_c</i>		390	440	...	279::	839:	0::	154:		
F04313-1649	<i>F</i>	0.219
	<i>EW</i>			53.4		
	<i>W</i>			642		
	<i>W_c</i>		0		
F05024-1941	<i>F</i>	0.0084:	0.21:	0.08::	0.067:	0.414	...	0.074::	0.102	2.13	1.57
	<i>EW</i>			6::	6.0:	38	...	7.5::	10.7		
	<i>W</i>			...	708::	862	640:		
	<i>W_c</i>		1380:	...	107::	503	0:		
F05156-3024	<i>F</i>	0.098	0.82	0.137:	0.089	1.34	0.143	0.160	0.97	1.45
	<i>EW</i>			11.8:	7.6	119	14.7	17.7		
	<i>W</i>			580::	541:	715	657:	787:		
	<i>W_c</i>		950	0::	0:	144	0:	359:		

Table 3: Optical^a and Near-Infrared Line Measurements.

IRAS		H β_{nl}	H α_{nl}	[Fe II]	H $_2$	Pa α_{nl}	Pa α_{bl}	Br δ	H $_2$ 1.958	H $_2$	He I	H $_2$	Br γ	H α /H β	P
(1)	(2)	(3)	(4)	1.644 (5)	1.835 (6)	1.875 (7)	1.875 (8)	1.945 (9)	+ [Si VI] 1.962 (10)	2.033 (11)	2.058 (12)	2.121 (13)	(14)	(15)	
F11095-0237	<i>F</i>	0.109	0.64	...	0.153	1.23	...	0.069:	0.265	0.094:	0.037:	0.263	0.125:	0.62	
	<i>EW</i>			...	25.6	220	...	13.8:	53.7	19.2:	7.8:	59.0	29.0:		
	<i>W</i>			...	865	950	...	925::	818	823::	487::	740	1122::		
	<i>W_c</i>		320	...	431	583	...	541::	325	338::	0::	0	834::		
F11180+1623	<i>F</i>	0.029	0.29:	0.197:: ^c	0.051	0.544	...	0.037:	0.104	0.095:	...	1.21	
	<i>EW</i>			36.4::	12.9	137	...	10.8:	31.2	30.2:	...		
	<i>W</i>			...	796:	936	...	886::	787	787::	...		
	<i>W_c</i>		210	...	267:	560	...	471::	239	240::	...		
F11223-1244	<i>F</i>	0.004:	0.20	0.108	0.118	0.854	0.213	0.084:	2.68	
	<i>EW</i>			9.4	11.1	81.6	21.5	8.5:		
	<i>W</i>			672:	635:	695	729	561::		
	<i>W_c</i>		960	0:	0:	0	204	0::		
F11506+1331	<i>F</i>	0.047	0.47	3.26	...	0.186:	0.181:	...	0.175:	0.241:	0.278:	1.13	
	<i>EW</i>			215	...	12.9:	12.6:	...	12.5:	17.6:	20.7:		
	<i>W</i>			916	...	1149::	763::	...	718::	906::	901::		
	<i>W_c</i>		80:	526	...	871::	138::	...	0::	507::	500::		
F11582+3020	<i>F</i>	0.040	0.25	...	0.070::	0.560	0.120:	0.76	
	<i>EW</i>			...	10.8::	90.6	20.0:		
	<i>W</i>			676	969::		
	<i>W_c</i>		250	0	670::		
F12018+1941	<i>F</i>	...	0.182 ^d	...	0.088:	0.785	0.183	0.041::	...	0.290	
	<i>EW</i>			...	12.9:	120	30.6	6.9::	...	52.6	...		
	<i>W</i>			...	783::	841	886	996:	...		
	<i>W_c</i>		224::	381	471	655:	...		
F12032+1707	<i>F</i>	0.214	1.65	0.348	0.313	0.981	...	0.193	0.550	0.338	0.94	
	<i>EW</i>			54.6	63.0	205	...	46.1	133	92.1		
	<i>W</i>			824	924	851	...	1334:	817	1442:		
	<i>W_c</i>		580	342	540	402	...	1103:	323	1232:		

Table 3: Optical^a and Near-Infrared Line Measurements.

IRAS		H β_{nl}	H α_{nl}	[Fe II]	H $_2$	Pa α_{nl}	Pa α_{bl}	Br δ	H $_2$ 1.958	H $_2$	He I	H $_2$	Br γ	H $\alpha/H\beta$	F
(1)	(2)	(3)	(4)	1.644 (5)	1.835 (6)	1.875 (7)	1.875 (8)	1.945 (9)	+ [Si VI] 1.962 (10)	2.033 (11)	2.058 (12)	2.121 (13)	(14)	(15)	F
F12112+0305	<i>F</i>	0.104	0.80	2.01	...	0.085:	0.144:	0.098:	0.093:	0.141:	0.217:	0.92	
	<i>EW</i>			118	...	5.2:	9.1:	6.6:	6.4:	10.1:	15.7:		
	<i>W</i>			896	...	686::	725::	828::	458::	630::	670::		
	<i>W_c</i>		559	...	0::	191::	441::	0::	0::	0::		
F12447+3721	<i>F</i>	0.391	2.06:	0.161	...	1.62	...	0.130:	0.072:	0.222:	0.61	
	<i>EW</i>			41.4	...	543	...	5.2:	29.7:	84.0:		
	<i>W</i>			802:	...	727	...	1055::	632::	785::		
	<i>W_c</i>		190	283:	...	0	...	742::	0::	232::		
F13106-0922	<i>F</i>	0.0495	0.33	...	0.055:	0.323	...	0.035:	0.122	0.091	...	0.211:	...	0.76	
	<i>EW</i>			...	12.2:	75.8	...	9.1:	32.3	26.9	...	71.2:	...		
	<i>W</i>			...	801::	874	...	790::	712	854:	...	1201::	...		
	<i>W_c</i>		160	...	281::	448	...	250::	0	407:	...	938::	...		
F13305-1739	<i>F</i>	0.955	9.55:	...	0.264	1.73	1.48	0.249:	0.973	0.191	...	0.217:	0.155::	1.18:	
	<i>EW</i>			...	18.8	129	110	19.7:	79.0	16.5	...	19.8:	15.0::		
	<i>W</i>			...	1030:	1072	2991	1813::	1679	965:	...	616::	...		
	<i>W_c</i>		1200	...	707:	766	2896	1651::	1503	607:	...	0::	...		
F13428+5608 ^e	<i>F</i>	0.821	8.21	...	0.847:	8.84	...	0.700:	2.02	0.754	...	1.42	0.822	1.22	
	<i>EW</i>			...	12.8:	132	...	11.2:	32.9	12.7	...	24.9	14.7		
	<i>W</i>			...	976::	1168	...	1171::	1167	1153:	...	1078	1034:		
	<i>W_c</i>		480	...	625::	895	...	899::	894	876:	...	774	712:		
F13443+0802 NE	<i>F</i>	0.101	1.01	...	0.098:	1.00	0.167	1.22	
	<i>EW</i>			...	5.8:	60.2	11.4		
	<i>W</i>			...	810::	954	1038:		
	<i>W_c</i>		500	...	307::	590	717:		
F13443+0802 SW	<i>F</i>	0.025	0.36	0.211	0.133	0.104:	...	1.57	
	<i>EW</i>			59.6	40.5	35.0:	...		
	<i>W</i>			943	1455:	1094::	...		
	<i>W_c</i>		410	572	1246:	797::	...		

Table 3: Optical^a and Near-Infrared Line Measurements.

IRAS		H β_{nl}	H α_{nl}	[Fe II]	H $_2$	Pa α_{nl}	Pa α_{bl}	Br δ	H $_2$ 1.958	H $_2$	He I	H $_2$	Br γ	H α /H β	Pa α
(1)	(2)	(3)	(4)	1.644 (5)	1.835 (6)	1.875 (7)	1.875 (8)	1.945 (9)	+ [Si VI] 1.962 (10)	2.033 (11)	2.058 (12)	2.121 (13)	(14)	(15)	(16)
F13454–2956	<i>F</i>	0.0084	0.12	...	0.086:	1.28	...	0.064:	0.266	0.164:	0.076:	1.54	2.0
	<i>EW</i>			...	7.5:	114	...	6.1:	25.4	16.8:	8.0:		
	<i>W</i>			...	728::	917	...	676::	949	842::	523::		
	<i>W_c</i>		70:	...	0::	528	...	0::	582	383::	0::		
F13509+0442	<i>F</i>	0.125	1.14	2.41	...	0.190	0.146	...	0.188:	0.232:	0.192:	1.20	1.0
	<i>EW</i>			252	...	21.9	17.2	...	23.2:	30.6:	26.5:		
	<i>W</i>			875	...	842:	803:	...	1063::	1002::	700::		
	<i>W_c</i>		450	...	384:	287:	...	754::	665::	0::		
F14053–1958	<i>F</i>	0.026:	0.11:	0.225	0.31	1.0
	<i>EW</i>			71.5		
	<i>W</i>			848		
	<i>W_c</i>		420	397		
F14070+0525	<i>F</i>	0.0044	0.11	0.052:	...	0.236	0.131:	2.08	1.0
	<i>EW</i>			9.8:	...	55.5	35.9:		
	<i>W</i>			780::	...	702	813::		
	<i>W_c</i>		...	212::	...	0	315::		
F14394+5332	<i>F</i>	0.584	4.49	...	0.585	3.97	...	0.391	1.00	0.273	...	0.840	0.659:	0.93	1.0
	<i>EW</i>			...	25.9	184	...	19.0	49.7	13.7	...	47.0	38.4:		
	<i>W</i>			...	1060	1031	...	1336:	1026	760:	...	810	2319::		
	<i>W_c</i>		1870	...	750	708	...	1106:	700	120:	...	305	2195::		
F15250+3609	<i>F</i>	0.285	1.9	...	0.201:	3.13	...	0.240:	0.413	0.154:	0.241::	0.432	0.290	0.76	1.0
	<i>EW</i>			...	6.4:	103	...	8.6:	15.0	6.0:	9.6::	18.0	12.5		
	<i>W</i>			...	914::	937	...	1089::	845	735::	...	732	761		
	<i>W_c</i>		150	...	523::	562	...	790::	389	0::	...	0	131		
F16156+0146	<i>F</i>	0.125	0.78	...	0.110:	1.15	...	0.104::	0.226	0.194	0.054::	0.69	1.0
	<i>EW</i>			...	20.3:	213	...	19.8::	43.2	35.6	9.7::		
	<i>W</i>			...	961::	1190	1056	706	...		
	<i>W_c</i>		590	...	600::	925	743	0	...		

Table 3: Optical^a and Near-Infrared Line Measurements.

IRAS		H β_{nl}	H α_{nl}	[Fe II]	H $_2$	Pa α_{nl}	Pa α_{bl}	Br δ	H $_2$ 1.958	H $_2$	He I	H $_2$	Br γ	H α /H β
(1)	(2)	(3)	(4)	1.644 (5)	1.835 (6)	1.875 (7)	1.875 (8)	1.945 (9)	+ [Si VI] 1.962 (10)	2.033 (11)	2.058 (12)	2.121 (13)	(14)	(15)
F16300+1558	<i>F</i>	0.026	0.22	0.064:	...	0.560	0.119:	1.00
	<i>EW</i>			9.0:	...	93.8	22.2:	
	<i>W</i>			1027::	...	928	959::	
	<i>W_c</i>		120	701::	...	547	597::	
F17208–0014	<i>F</i>	0.086	1.6	6.21	...	0.692::	1.05	0.564:	0.285:	1.14	0.780	1.87
	<i>EW</i>			90.7	...	10.5::	16.2	9.0:	4.6:	19.2	13.5	
	<i>W</i>			918	806	932::	798::	759	794	
	<i>W_c</i>		529	294	553::	273::	114	260	
F22491–1808	<i>F</i>	0.368	2.3	...	0.049:	0.719	0.110:	0.81
	<i>EW</i>			...	4.2:	64.8	10.9:	
	<i>W</i>			...	565::	882	1138::	
	<i>W_c</i>		0::	536	898::	
F23365+3604	<i>F</i>	0.208	1.6	...	0.372:	4.94	0.468	0.468	0.357	0.88
	<i>EW</i>			...	9.9:	134	13.5	15.3	12.0	
	<i>W</i>			...	874::	927	777:	800:	683:	
	<i>W_c</i>		260	...	524::	607	337:	388:	0:	
F11058–1131 (LIG)	<i>F</i>	2.64 ^f	13.9 ^f	...	0.302:	2.27	6.94	...	0.585	0.14:	0.14:	0.49
	<i>EW</i>			...	3.2:	24.3	74.3	...	0.64	1.6:	1.6:	
	<i>W</i>			...	1097::	903	7218	...	934	835::	684::	
	<i>W_c</i>		220 ^f	...	801::	503	7179	...	557	368::	0::	

Note. — Meaning of columns and rows:

Column (1) – Name of object.

Column (2) – Meaning of rows. We list the observed line flux (10^{-14} ergs s^{-1} cm^{-2}) on the first row, the observed equivalent width (\AA) on the second row, the observed line width ($km\ s^{-1}$) on the third row, and the line width corrected for the instrumental resolution ($km\ s^{-1}$) on the fourth row.

Columns (3) – (14) – Line fluxes, equivalent widths, and line widths for narrow $H\beta$, narrow $H\alpha$, $[Fe\ II]\ \lambda 1.644$, $H_2\ \lambda 1.835$, narrow $Pa\alpha$, broad $Pa\alpha$, $Br\delta$, the blend of $H_2\ \lambda 1.958$ and $[Si\ VI]\ \lambda 1.962$, $H_2\ \lambda 2.033$, $He\ I\ \lambda 2.058$, $H_2\ \lambda 2.122$, and narrow $Br\gamma$, respectively.

Column (15) – (17) – The color excesses derived from $H\alpha/H\beta$ were taken directly from Kim et al. (1998) or Veilleux et al. (1999). The infrared color excesses were derived using

$$E(B - V)(\text{line 2/line 1}) = \frac{2.5}{\frac{A_1}{E(B-V)} + \frac{A_2}{E(B-V)}} \log \left[\frac{\left(\frac{F_2}{F_1}\right)}{\left(\frac{F_2}{F_1}\right)_0} \right]$$

with the intrinsic flux ratios and interstellar extinction coefficients listed in Table 2 of Veilleux et al. (1997a). The reddenings enclosed in parentheses were calculated using the sum of the broad and narrow-line fluxes; they should therefore be considered upper limits to the actual values.

^a Unless otherwise noted, all of the optical measurements are from Kim et al. (1995, 1998) or Veilleux et al. (1995, 1999).

^b Observed fluxes (10^{-14} erg s^{-1} cm^{-2}), equivalent widths (\AA), observed line widths ($km\ s^{-1}$), and corrected line widths ($km\ s^{-1}$) for other lines: $He\ I_{nl}\ \lambda 1.083 = 1.99, 6.6, 753, 456$; $He\ I_{bl}\ \lambda 1.083 = 11.3, 38, 6171, \text{ and } 6142$; $Pa\beta_{nl} = 7.34, 20.0, 1687, \text{ and } 1577$; $Pa\beta_{bl} = 3.2, 8.8, 8936, \text{ and } 8916$; The color excess derived from $Pa\beta_{nl}/H\alpha_{nl}$ is 2.60.

^c Line affected by atmospheric correction?

^d From Armus et al. (1989)

^e Observed fluxes (10^{-14} erg s^{-1} cm^{-2}), equivalent widths (\AA), observed line widths ($km\ s^{-1}$), and corrected line widths ($km\ s^{-1}$) for other lines: $He\ I_{nl}\ \lambda 1.083 = 3.21, 49.9, 1108, \text{ and } 897$; $[Fe\ II]\ \lambda 1.256 = 1.50, 45.0, 939, \text{ and } 677$; $Pa\beta_{nl} = 1.35, 40.0, 718, \text{ and } 306$; The color excess derived from $Pa\beta_{nl}/H\alpha_{nl}$ is 0.77.

^f From Osterbrock & De Robertis (1985). The corrected line width refers to narrow $H\alpha$ rather than $[O\ III]\ \lambda 0.5007$.

REFERENCES

- Antonucci, R. 1993, *ARA&A*, 31, 473
- Armus, L., Heckman, T. M., & Miley, G. K. 1988, *ApJ*, 326, L45
- Elvis, M. et al. 1994, *ApJS*, 95, 1
- Genzel, R., et al. 1998, *ApJ*, 498, 579
- Goldader, J. D., Joseph, R. D., Doyon, R., & Sanders, D. B. 1995, *ApJ*, 444, 97
- . 1997a, *ApJS*, 108, 449
- . 1997b, *ApJ*, 474, 104
- Goodrich, R. W., Veilleux, S., & Hill, G. J. 1994, *ApJ*, 422, 521
- Helou, G., Kahn, I. R., Malek, L., & Boehmer, L. 1988, *ApJS*, 68, 151
- Kim, D.-C. 1995, Ph.D. Thesis, University of Hawaii
- Kim, D.-C., & Sanders, D. B. 1998, *ApJS*, 119, 41
- Kim, D.-C., Sanders, D. B., Veilleux, S., Mazzarella, J. M., & Soifer, B. T. 1995, *ApJS*, 98, 129
- Kim, D.-C., Veilleux, S., & Sanders, D. B. 1998, *ApJ*, 508, 627
- Lutz, D., Veilleux, S., & Genzel, R. 1999, *ApJ*, submitted
- Marconi, A., Moorwood, A. F. M., Salvati, M., & Oliva, E. 1994, *A&A*, 291, 18
- Moshir, M., et al. 1992, Explanatory Supplement to the IRAS Faint Source Survey, Version 2, JPL D-10015 8/92 (Pasadena: JPL) (FSC)
- Mountain, C. M., Robertson, D. J., Lee, T. J., & Wade, R. 1990, *Instrumentation in Astronomy VII*, ed. D. L. Crawford (Proc. SPIE, Vol. 1235), 25
- Mulchaey, J. S., et al. 1994, *ApJ*, 436, 586
- Osterbrock, D. E., & de Robertis, M. M. 1985, *PASP*, 97, 1129
- Sanders, D. B., & Mirabel, I. F. 1996, *ARA&A*, 34, 725
- Sanders, D. B., Phinney, E. S., Neugebauer, G., & Matthews, K. 1989, *ApJ*, 347, 29
- Sanders, D. B., Soifer, B. T., Elias, J. H., Madore, B. F., Matthews, K., Neugebauer, G., & Scoville, N. Z. 1988a, *ApJ*, 325, 74
- Veilleux, S., Goodrich, R. W., & Hill, G. J. 1997a, *ApJ*, 477, 631
- Veilleux, S., Kim, D.-C., & Sanders, D. B. 1999, *ApJ*, submitted (VKS)
- Veilleux, S., Kim, D.-C., Sanders, D. B., Mazzarella, J. M., & Soifer, B. T. 1995, *ApJS*, 98, 171
- Veilleux, S., Sanders, D. B., & Kim, D.-C. 1997b, *ApJ*, 484, 92
- Ward, M. J., Blanco, P. R., Wilson, A. S., & Nishida, M. 1991, *ApJ*, 382, 115
- Yee, H. K. C. 1980, *ApJ*, 241, 894

Young, S., Hough, J. H., Bailey, J. A., Axon, D. J., & Ward, M. J. 1993, MNRAS, 260, L1

Fig. 1.— Reduced near-infrared spectra of the *IRAS* ultraluminous infrared galaxies in the new sample. f_λ is plotted versus $\lambda_{\text{observed}}$. The units of the vertical axis are 10^{-11} ergs $\text{s}^{-1} \text{cm}^{-2} \mu\text{m}^{-1}$, while the wavelength scale is in μm .

Fig. 2.— Distributions of the (a) $\text{H}_2 \lambda 1.958/\text{Pa}\alpha_{nl}$ and (b) $\text{H}_2 \lambda 2.122/\text{Pa}\alpha_{nl}$ flux ratios for the optically classified H II galaxies (dotted line), LINERs (dashed line), and Seyfert 2 galaxies (solid line) of the combined sample.

Fig. 3.— Luminosity of $\text{Pa}\alpha$ as a function of the infrared luminosity in units of the solar bolometric luminosity, 3.83×10^{33} erg s^{-1} . The vertical axis of panels (a) and (b) shows the luminosities in the narrow component of $\text{Pa}\alpha$ while the luminosities plotted in panels (c) and (d) refer to the sum of the narrow and broad components. Dereddening of the emission-line luminosities in the left and right panels was carried out using the color excesses derived from the optical and infrared line ratios, respectively. Ultraluminous infrared galaxies with obscured BLRs detected in our near-infrared spectra are represented by filled boxes, Seyfert 2 galaxies by filled circles, LINERs by open circles, and H II galaxies by asterisks. The filled triangle is the luminous infrared galaxy F11058-1131. The solid line represents the relation found by Goldader et al. (1995, 1997a,b) for lower luminosity infrared galaxies after assuming a $\text{Pa}\alpha/\text{Br}\gamma$ flux ratio of 12 (case B recombination). Several data points fall below the solid line, therefore suggesting a $\text{Pa}\alpha$ emission deficit in many of these objects.

Fig. 4.— Ratios of the dereddened $\text{Pa}\alpha$ and infrared luminosities as a function of the *IRAS* f_{25}/f_{60} ratio. Dereddening was carried out using (a) the optical line ratios and (b) the infrared line ratios. Meaning of the symbols is the same as in Fig. 3. The $\text{Pa}\alpha$ -to-IR luminosity ratio is on average larger in those objects with ‘warm’ infrared colors ($f_{25}/f_{60} > 0.2$).

Fig. 5.— Comparison of the $\text{H}\beta$ luminosities of optical and obscured BLRs in infrared galaxies and optically identified QSOs as a function of their bolometric luminosities. L_{bol} for the QSOs was determined using the bolometric correction factor 11.8 (i.e. $L_{\text{bol}} = 11.8\nu_B L_\nu(B)$): Elvis et al. 1994; Sanders & Mirabel 1996), except for those few sources that were detected by *IRAS*, in which case L_{bol} was taken from Sanders et al. (1989). For the ULIGs L_{bol} was taken to be $1.15 \times L_{\text{IR}}$ (Kim & Sanders 1998). The $\text{H}\beta$ data for the optically selected QSOs are from Yee (1980) corrected for $H_0 = 75 \text{ km s}^{-1} \text{Mpc}^{-1}$ and $q_0 = 0$. The broad $\text{H}\beta$ luminosities of the infrared galaxies were calculated from the measured broad $\text{Pa}\alpha$ fluxes assuming case B recombination (except for Mrk 463E where the broad $\text{Pa}\beta$ flux was used). The reddening correction was carried out using the color excesses derived from the infrared line ratios. Most of the infrared galaxies fall close to the quasar relation (solid line).

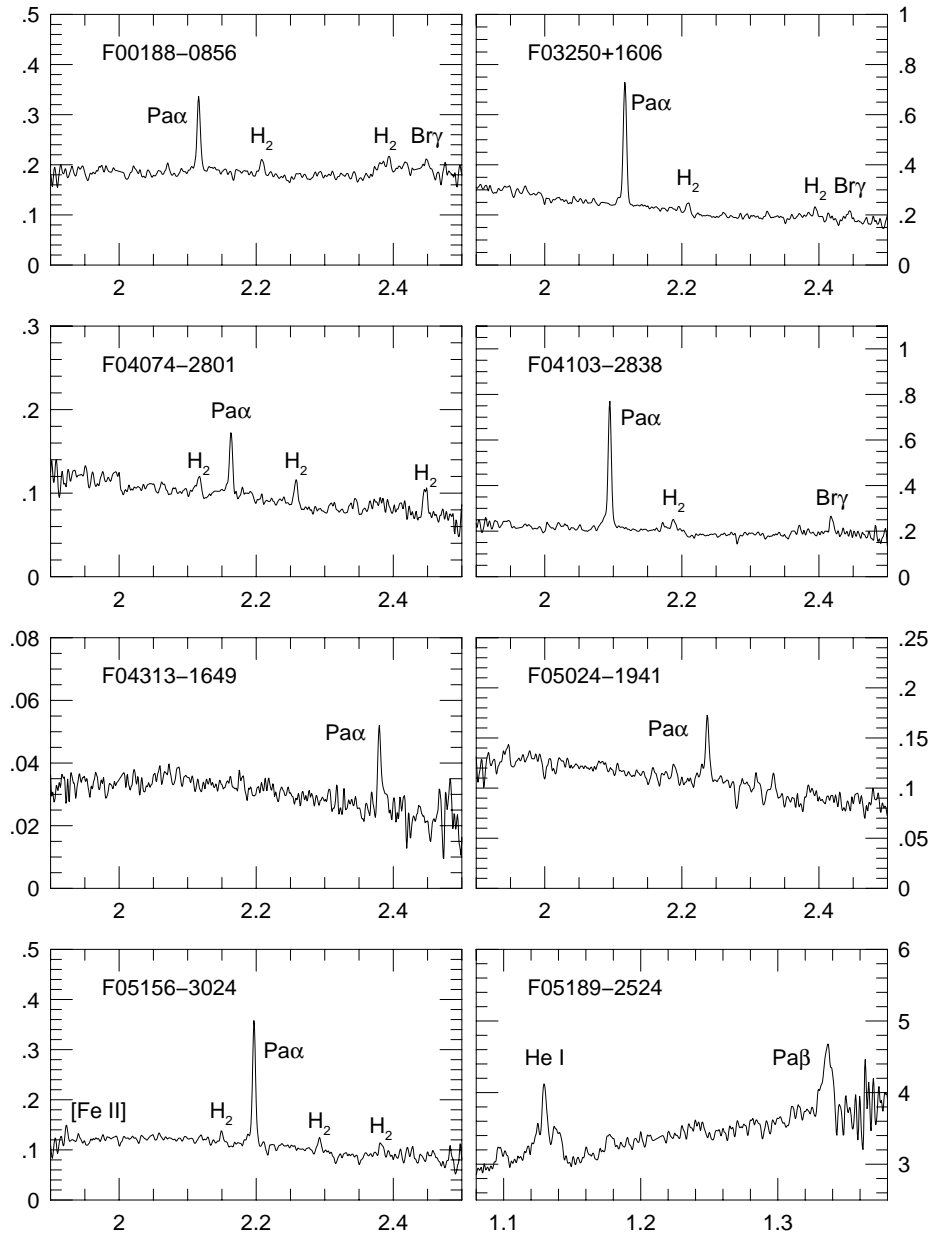


Fig. 1.—

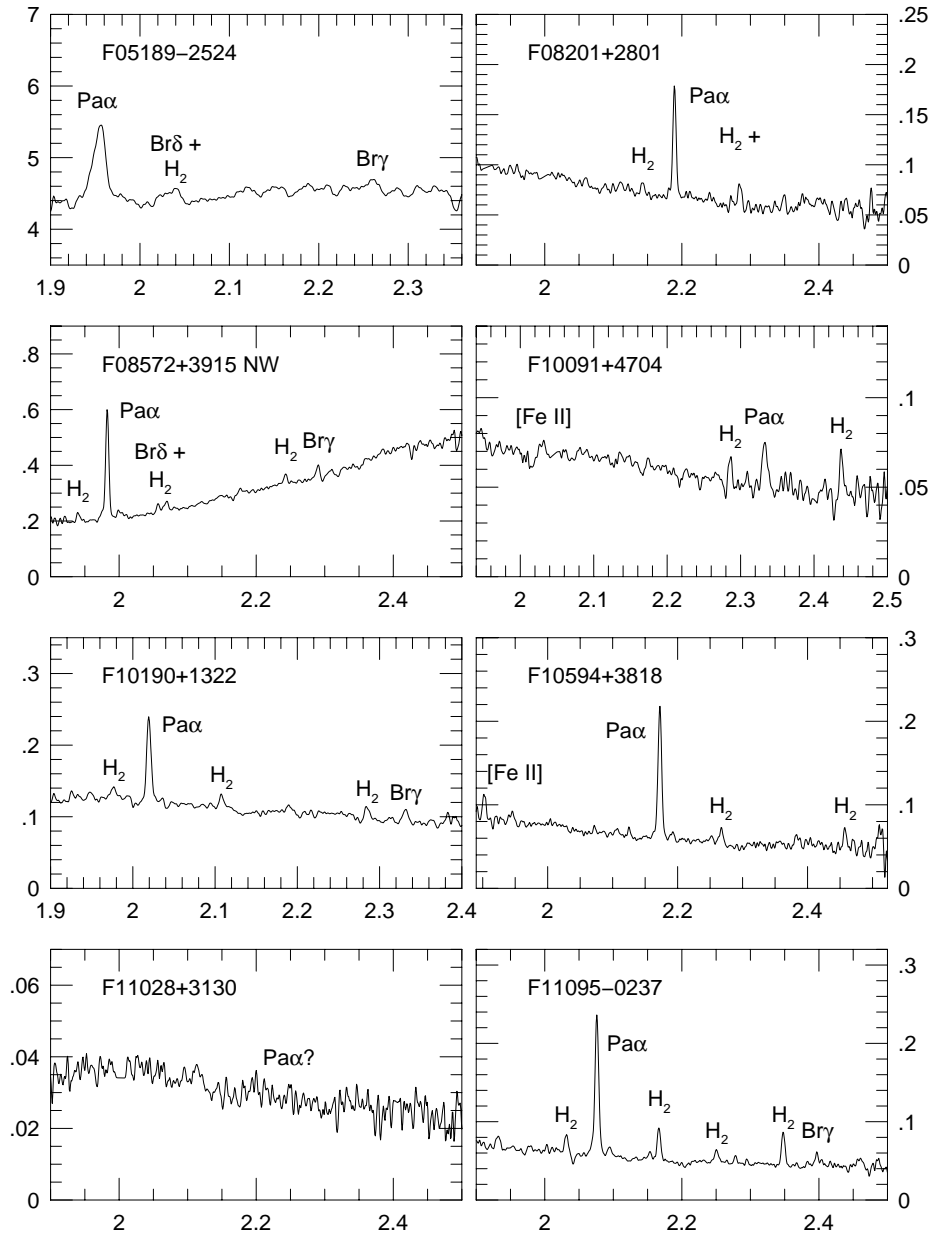


Fig. 1.—

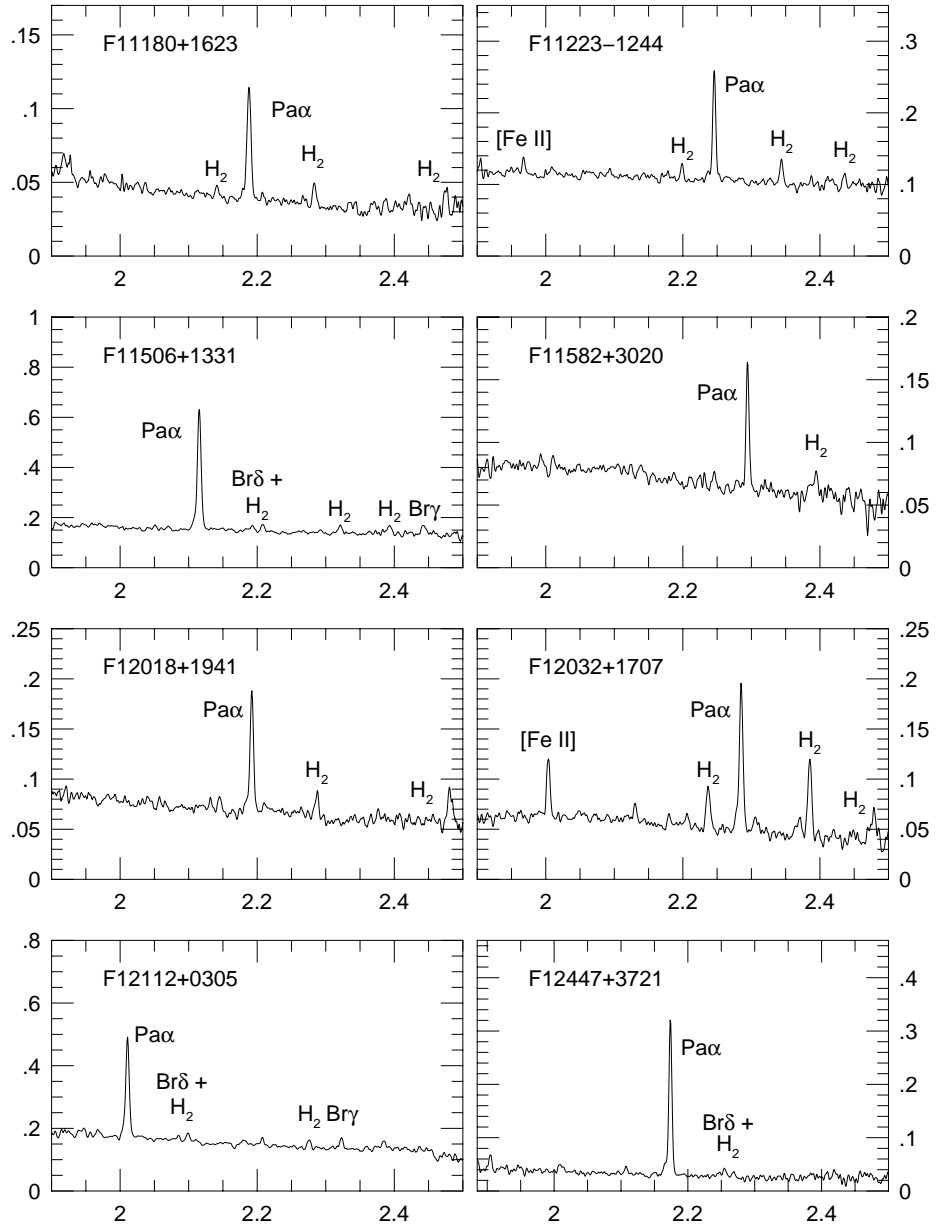


Fig. 1.—

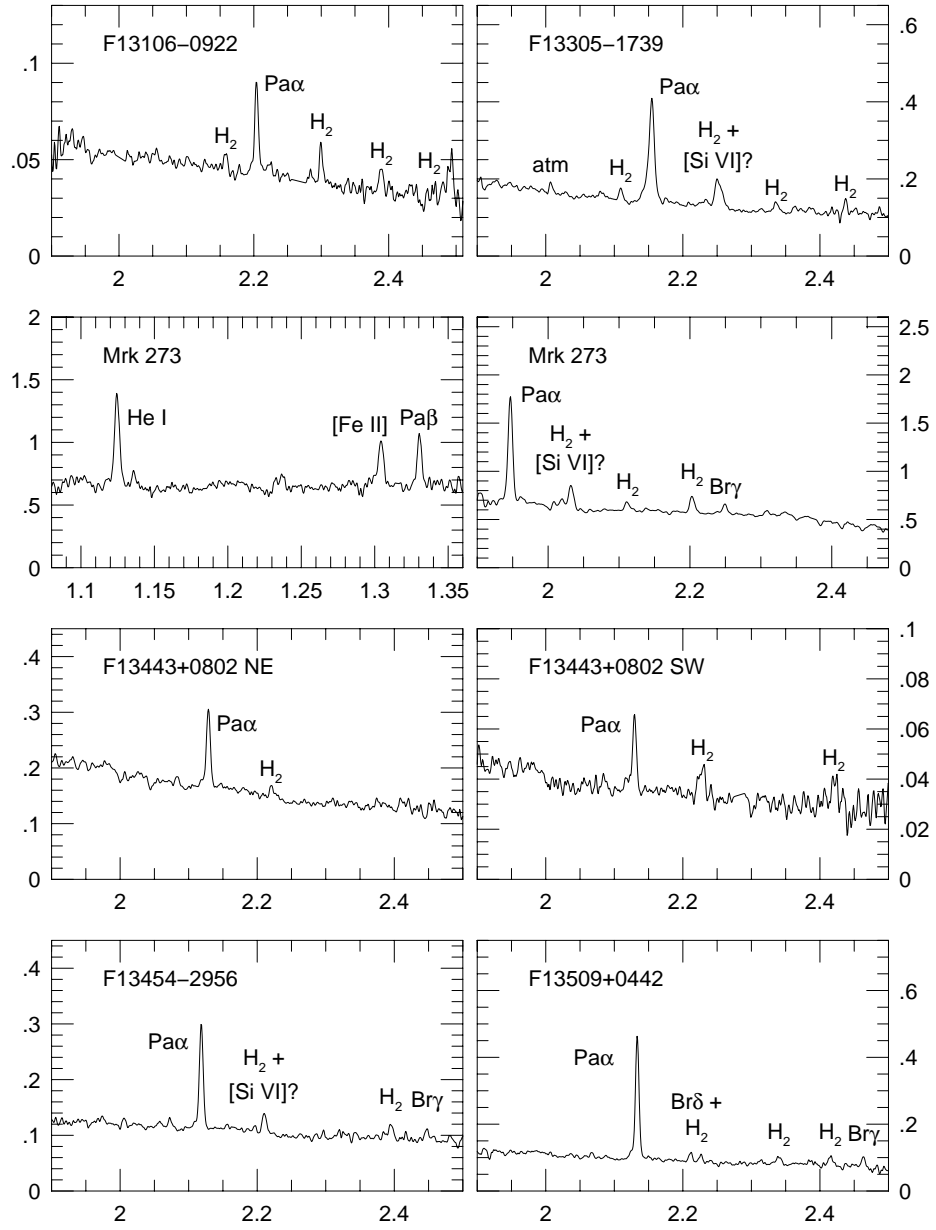


Fig. 1.—

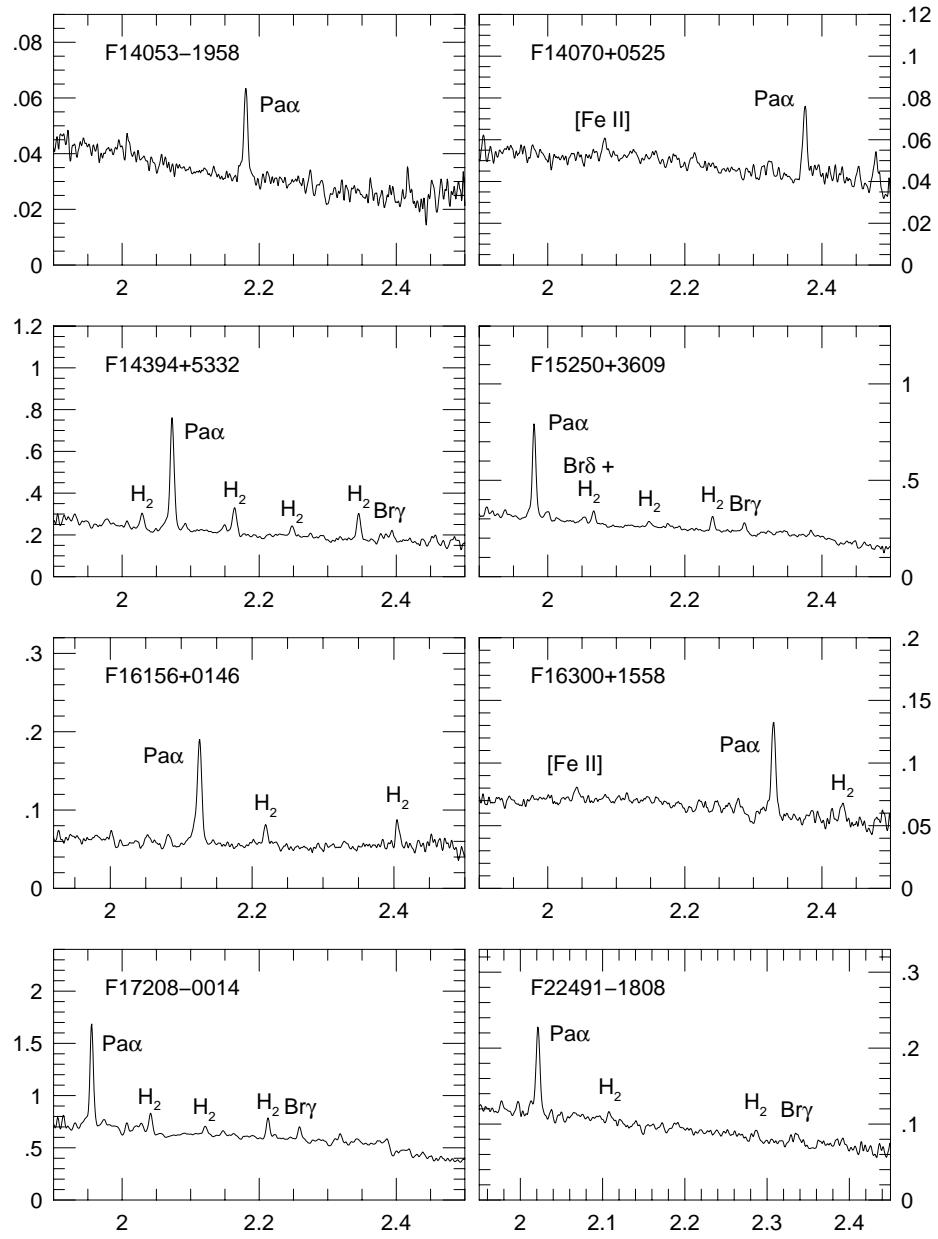


Fig. 1.—

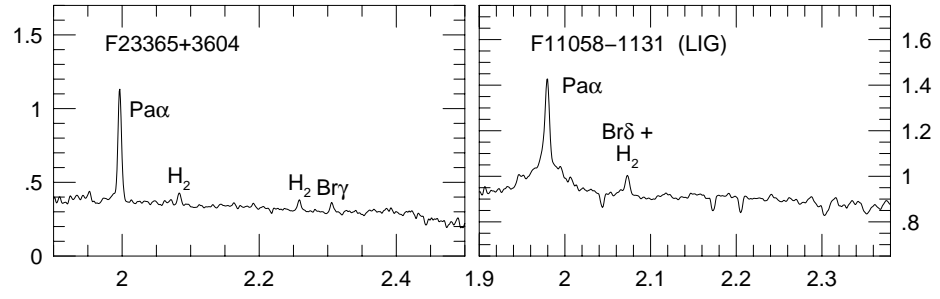


Fig. 1.—

Fig. 2.—

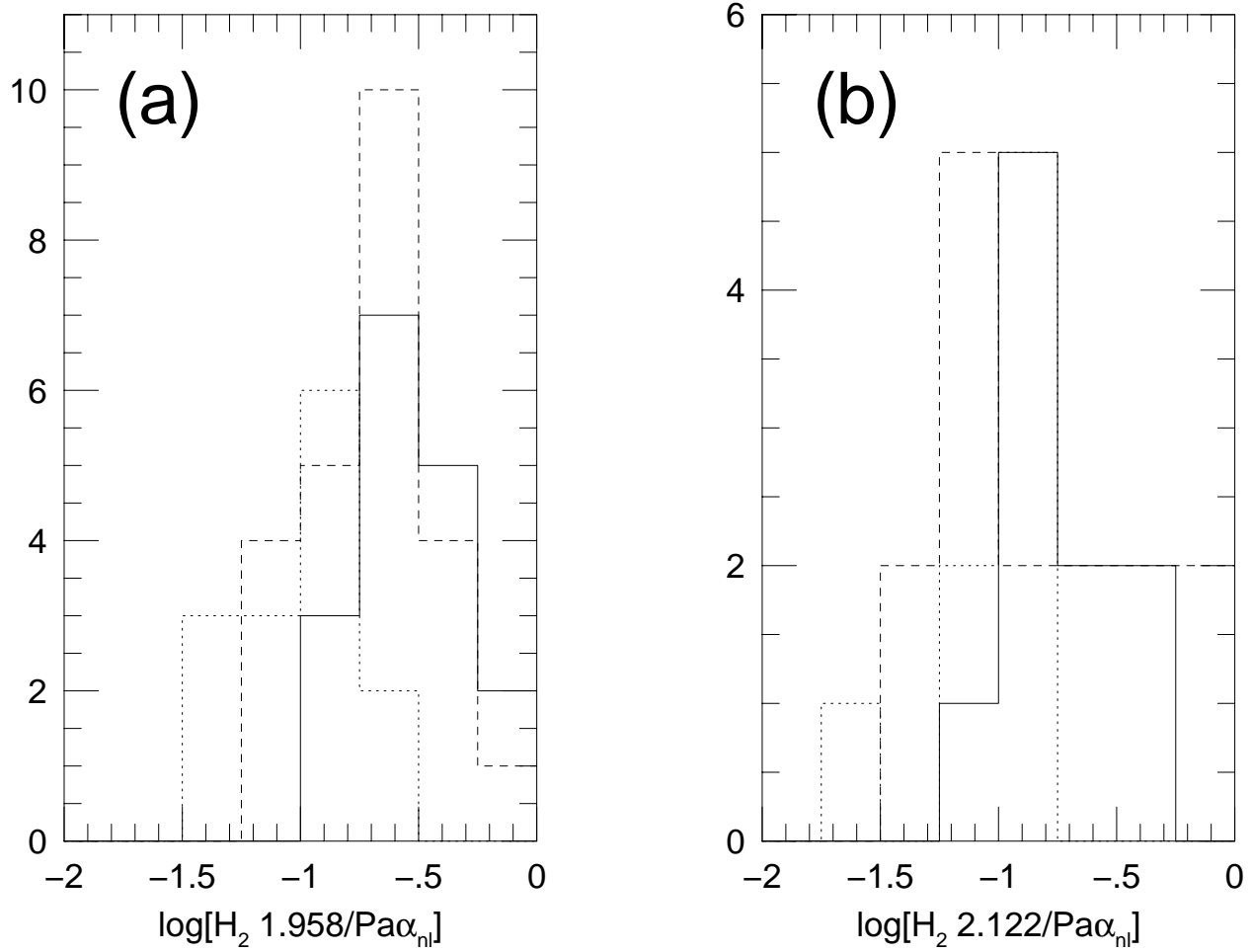
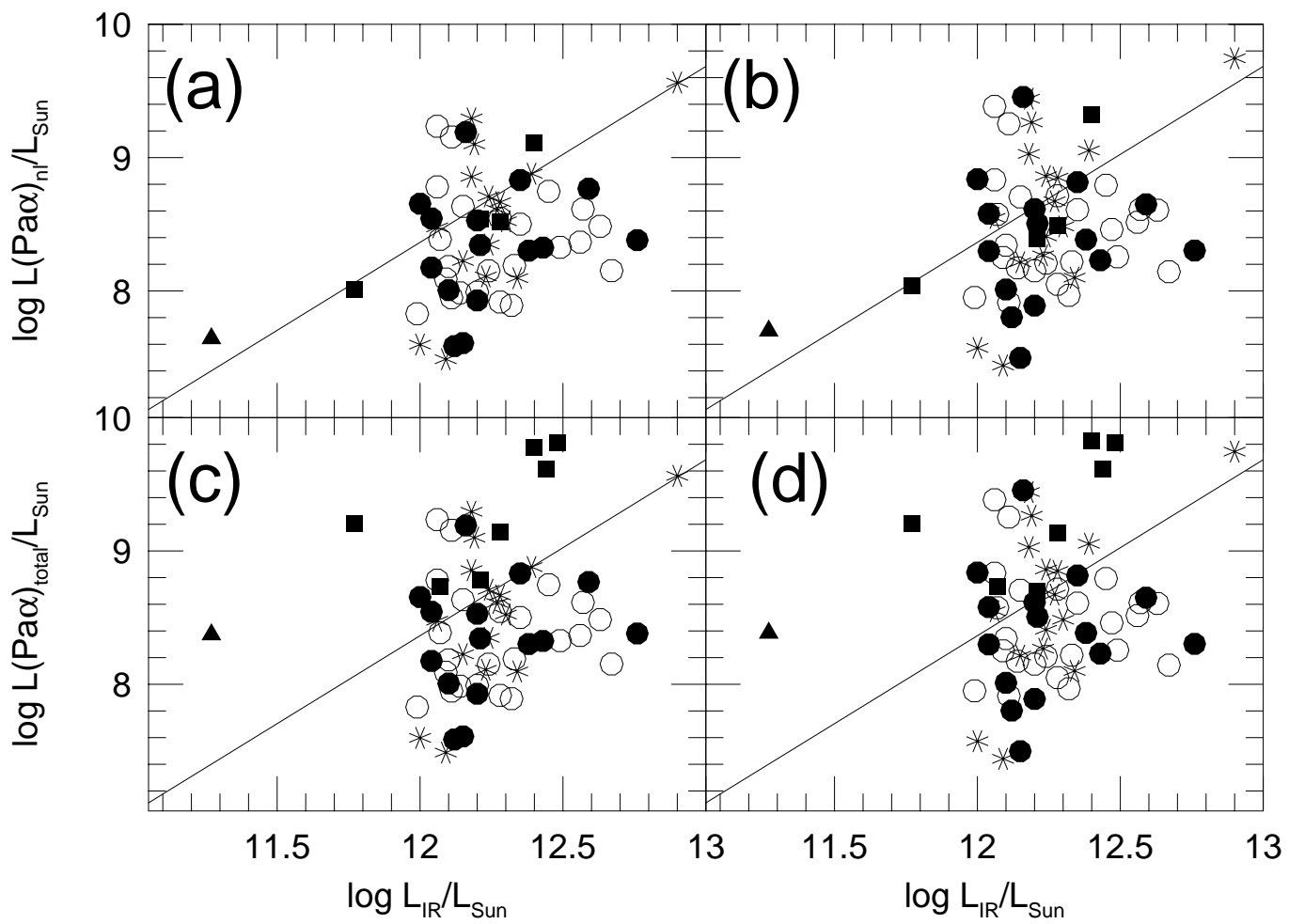


Fig. 3.—



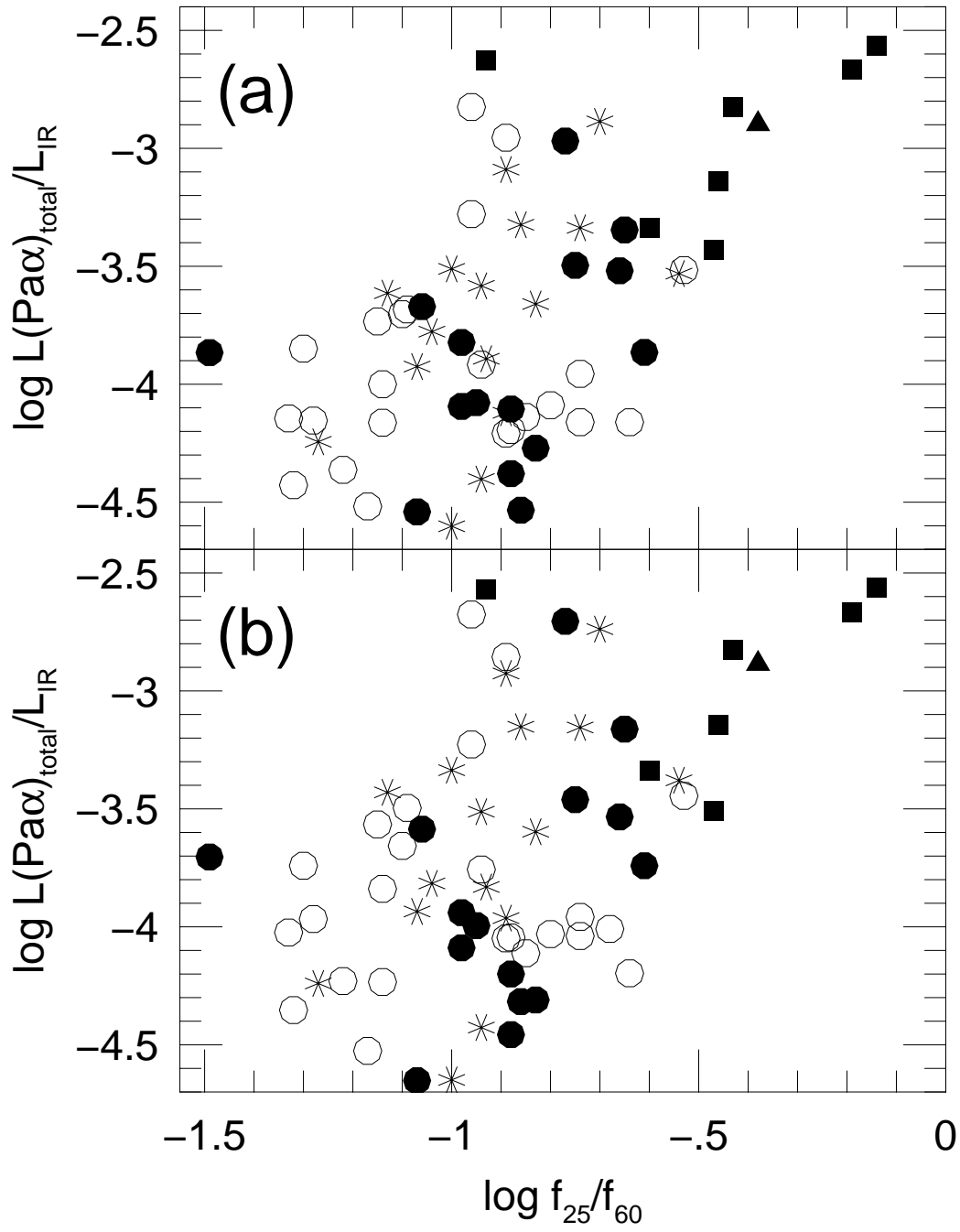


Fig. 4.—

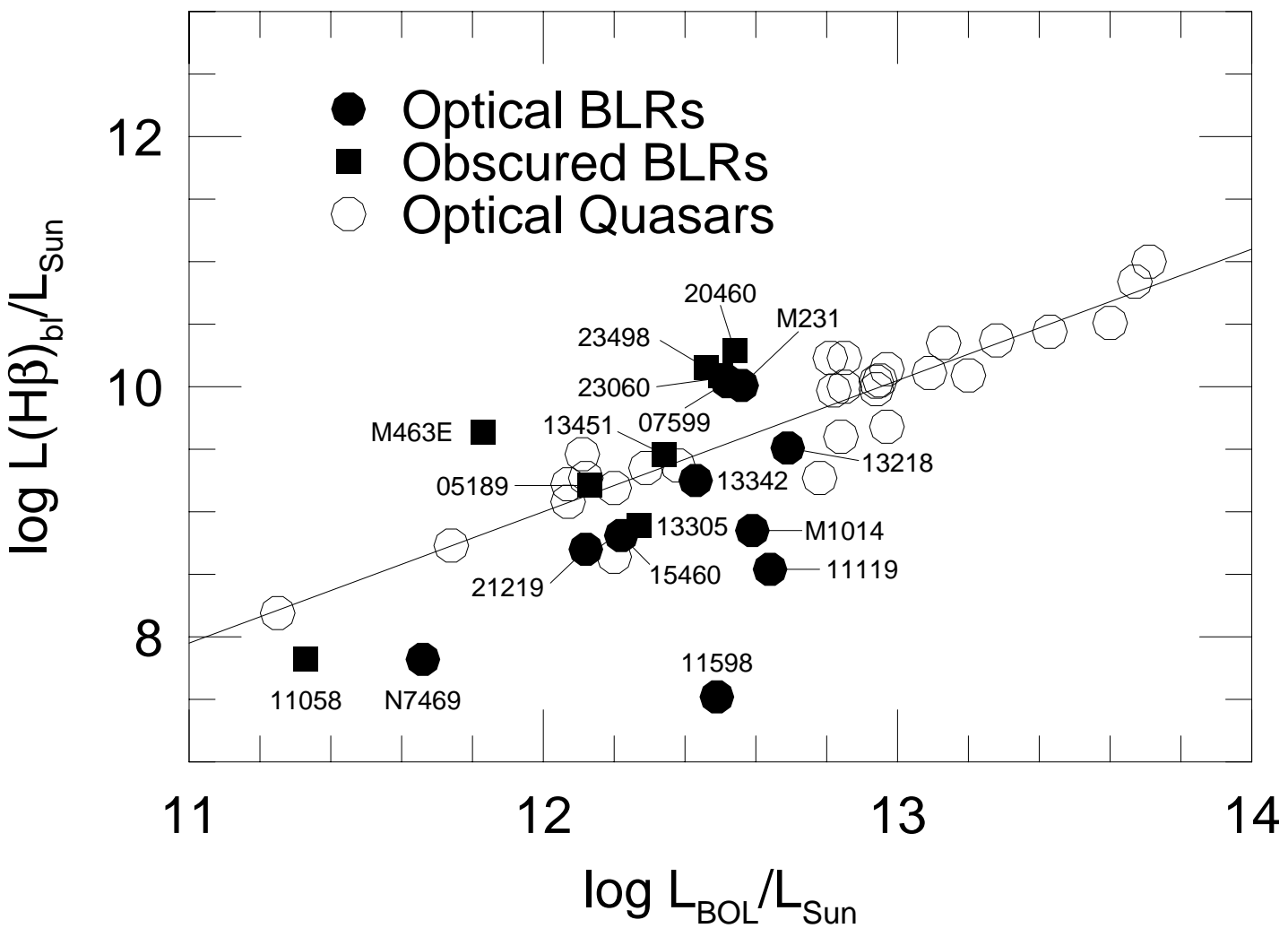


Fig. 5.—